

Lithospheric structure of the Labrador Sea from constrained 3-D gravity inversion

J. Kim Welford and Jeremy Hall

Department of Earth Sciences, Memorial University of Newfoundland, St. John's, NL, Canada. E-mail: kwelford@mun.ca

Accepted 2013 July 22. Received 2013 July 22; in original form 2012 December 13

SUMMARY

Regional inversions of free air gravity data constrained by bathymetric and sediment thickness information were undertaken over the Labrador Sea and its margins to generate 3-D density anomaly models to investigate broad-scale crustal structural variations across the extinct spreading centre. Benchmarked against independent seismic Moho depth constraints, a density anomaly isosurface within the inverted volumes was selected as a Moho-proxy and regional maps of Moho structure were developed. Inversions using two different sources for depth to basement constraints revealed similar Moho structures with a depth to Moho of 12 km beneath the Labrador Sea which deepens to 20 km and greater towards Davis Strait and beneath the offshore extension of the Grenville Province. Density anomaly slices through the models corresponding to seismic lines show good agreement between the inverted Moho-proxy and the seismic Moho, with the only exceptions occurring where a high velocity lower crustal zone or underplate has been modelled from wide-angle reflection/refraction profiling studies. The inverted depth to Moho estimates were combined with depth to basement constraints to investigate crustal thickness, both for the full crust and for individual crustal layers, revealing that the crust of the Labrador Sea is generally 5–10 km thick but thickens to 20–25 km towards Davis Strait and beneath the offshore extension of the Grenville Province, not taking into account high density underplates or anomalously high density lower crust. Sediment and crustal thickness variations were investigated to compute stretching factors, β , across the Labrador Sea and to identify zones which deviate from local isostatic compensation. Assuming both an initial unstretched crustal thickness of 35 km and using a variable unstretched crustal thickness model, much of the Labrador Sea has experienced 70–90 per cent thinning. The derived β values suggest that embrittlement of the entire crust and serpentinization of the upper mantle are likely to have occurred for large portions of the central and southern Labrador Sea, inboard of known oceanic crust. Isostatic considerations reveal sediment excess and deficiency on the Labrador and Greenland margins, respectively, possibly reflecting fundamental rheological asymmetry, with the Greenland margin appearing weaker than the Labrador margin. A strong gradient from sediment deficiency to excess, exclusive to the Labrador margin, may reveal the southwestern limit of a regional graben bounding listric detachment or of a zone of distributed faults and detachments.

Key words: Inverse theory; Gravity anomalies and Earth structure; Continental tectonics: extensional; Crustal structure.

1 INTRODUCTION

The Labrador Sea between Labrador, Canada and Greenland includes an extinct spreading centre that represents an ideal research target for studies of extensional non-volcanic/magma-poor margins because the entire system is spatially constrained and all components of a non-volcanic margin, namely thinned continental crust, oceanic crust and transitional crust possibly containing exhumed

serpentinized mantle material, are present. To complement existing seismic studies of the Labrador Sea, 3-D gravity inversions constrained by regional bathymetric and depth to basement estimates were undertaken to assess lithospheric density structure, Moho depth and crustal thickness across the entire sea. From these, the transition from a non-volcanic to a volcanic margin farther north is investigated and stretching (β) factors are extracted to help explain the evolution of the Labrador Sea as a whole and to better

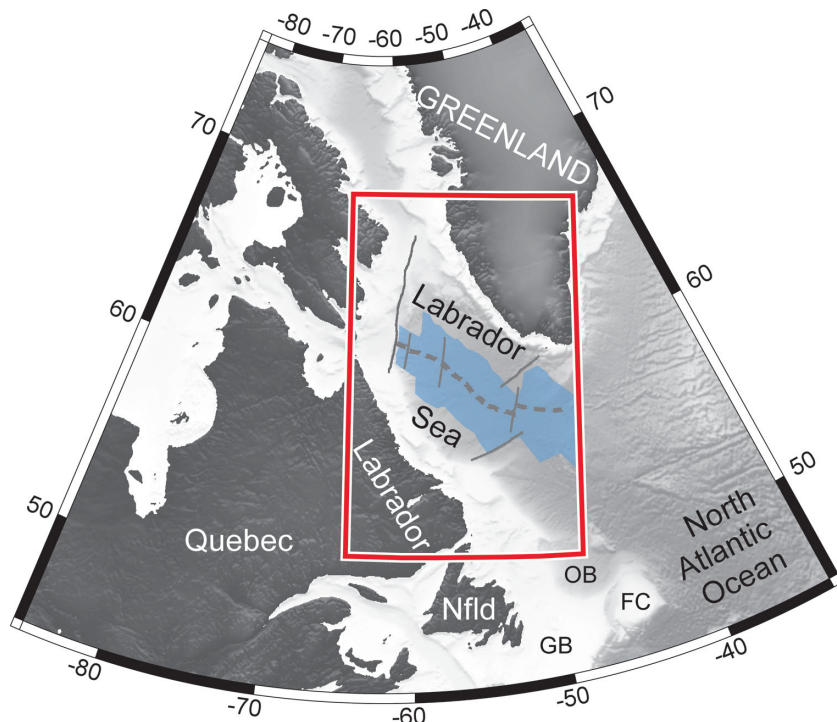


Figure 1. Bathymetric map of the Labrador Sea and its environs. The red box outlines the study region and the area used for the constrained 3-D gravity inversion. The locations of the extinct rift (dashed grey line), key fracture zones (thin solid grey lines), and interpreted extent of oceanic crust [blue shaded area (Chalmers & Pulvertaft 2001)] within the Labrador Sea are plotted for reference. FC, Flemish Cap; GB, Grand Banks; Nfld, Newfoundland; OB, Orphan Basin.

understand the evolution of the Saglek and Hopedale basins on the Labrador Shelf.

2 TECTONIC SETTING

The Labrador Sea includes the extinct spreading centre that separated Greenland from North America (Fig. 1). While crustal stretching began at 130 Ma (Roest & Srivastava 1989) and continued until 62 Ma (magnetic chron 28) with earlier magnetic lineaments (magnetic chron 33 to 28) caused by serpentinization and possible exhumation of the mantle, seafloor spreading developed from south to north in the Early Tertiary from 61 to 56 Ma (magnetic chron 27 to 25; Chalmers & Laursen 1995) until a triple junction developed south of Greenland and seafloor spreading eventually flipped entirely to the eastern margin of Greenland at 36 Ma (Roest & Srivastava 1989). With the reorientation and relocation of the spreading centre, spreading within the Labrador Sea became oblique, slowed and eventually ceased between 45 Ma (magnetic chron 20) and 36 Ma (magnetic chron 13). The relocation of the spreading centre east of Greenland coincided temporally with separation of Rockall Bank from Greenland, separation of the Barents Shelf from Lomonosov Ridge in the Arctic, spreading in the Norwegian-Greenland Sea and Eurasian Basin as well as basalt extrusion on the east and west coasts of Greenland (Roest & Srivastava 1989).

The tectonic evolution and plate kinematics of the Labrador Sea and its margins have been deduced largely from magnetic anomalies (Kristoffersen & Talwani 1977; Srivastava 1978; Roest & Srivastava 1989) but also from targeted seismic reflection and refraction experiments (Chian & Louden 1992; Osler & Louden 1992, 1995; Chian & Louden 1994; Keen *et al.* 1994; Chian *et al.* 1995a,b; Reid 1996; Funck & Louden 1998, 1999, 2000; Funck *et al.* 2001b, 2007, 2008;

Gerlings *et al.* 2009). Magnetic anomalies are well developed in the southern Labrador Sea but become less clear and interpretable in the north. Nonetheless, these anomalies (plus corresponding gravity anomalies and key seismic profiles) reveal complex fracturing in the Labrador Sea with three main fracture zones (Minna, Snorri and Hudson; Fig. 2) offsetting magnetic anomalies 20–24 (Srivastava 1978). The older Cartwright Fracture Zone on the Labrador margin represents the western extension of the Julian Haab Fracture Zone on the Greenland margin (Fig. 2) and these roughly correspond with the offshore extension of the Grenville Front (Srivastava 1978; Roest & Srivastava 1989) and may be inherited from that orogeny.

Rifting between Greenland and Labrador was asymmetrical with rifting initially focused closer to the Greenland margin before gradually migrating westward after the formation of anomaly 32 (72 Ma) in the Late Cretaceous (Srivastava & Roest 1999). Consequently, there is a wider zone of thinned continental crust on the Labrador margin compared to the Greenland margin. In addition to oceanic crust along the axis of the Labrador Sea, thinned continental crust underlain by serpentinized mantle has been inferred within the transition zones of both the Labrador and Greenland margins from seismic refraction velocity models (van der Linden 1975; Chian & Louden 1994; Chian *et al.* 1995a,b; Louden *et al.* 1996).

3 SEDIMENTARY BASIN ARCHITECTURE

The distribution of sedimentary basins in the Labrador Sea is highly asymmetric. Offshore Greenland has only minor basins while the Labrador Shelf is dominated by two large Mesozoic sedimentary basins with NNW–SSE trends, underlain by crystalline Precambrian rocks, namely the Saglek Basin in the north and the Hopedale Basin in the south (Fig. 2). A recent regional long-offset 2-D seismic

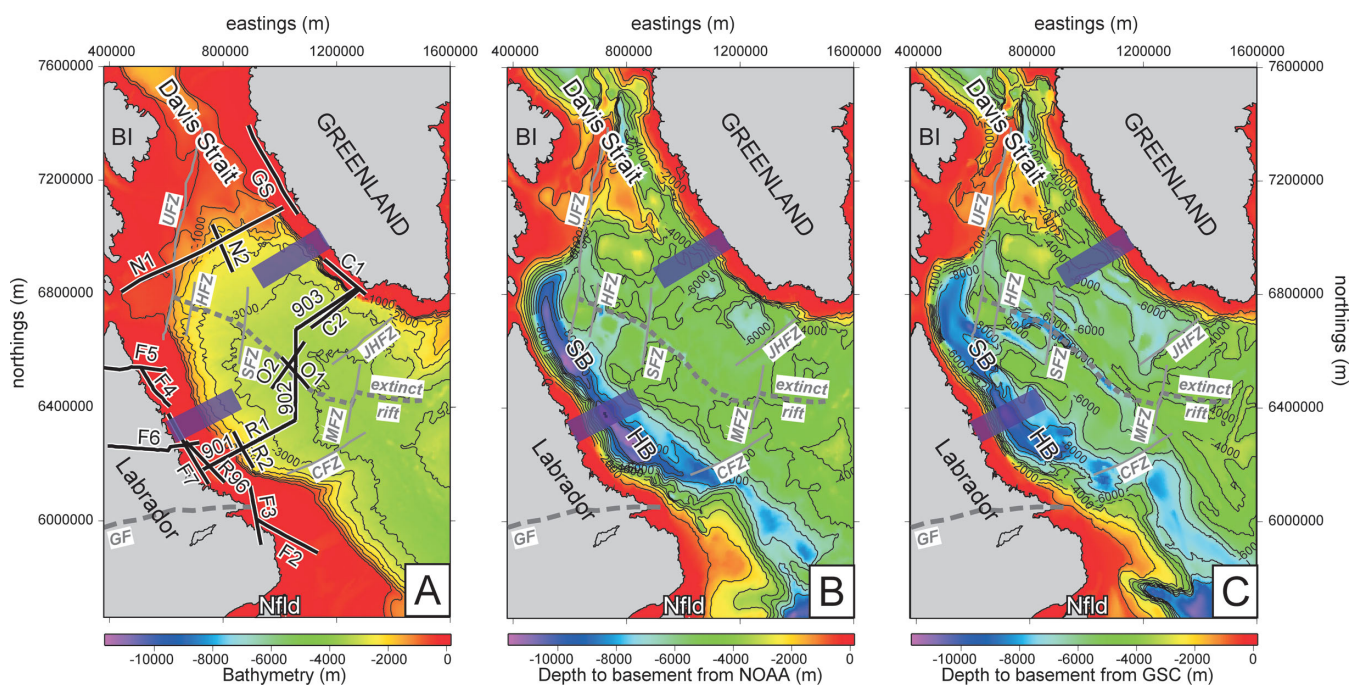


Figure 2. Maps of bathymetry (a) and depth to basement derived from the NOAA sediment thickness estimates (b; Divins 2003) and from the Geological Survey of Canada (GSC) compilation (c; Oakey & Stark 1995). Key published deep seismic lines are plotted with the solid black lines in panel (a), see text for line label references. The locations of the extinct rift (dashed grey line) and fracture zones (thin solid grey lines) within the Labrador Sea are plotted on all panels for reference. The purple boxes on all the panels show the location of the non-volcanic to volcanic transition on both margins proposed by Keen *et al.* (2012). BI, Baffin Island; CFZ, Cartwright Fracture Zone; GF, Grenville Front; HB, Hopedale Basin; HFZ, Hudson Fracture Zone; JHFZ, Julian Haab Fracture Zone; MFZ, Minna Fracture Zone; Nfld, Newfoundland; SB, Saglek Basin; SFZ, Snorri Fracture Zone; UFZ, Ungava Fault Zone.

survey in the Labrador Sea has now also identified a number of previously unrecognized extensive Mesozoic basins across the slope and into deep water (Carter *et al.* 2013). Dickie *et al.* (2011) provide the most up-to-date tectonostratigraphic chart for the Labrador Shelf consisting of seven main units. To summarize the work of Dickie *et al.* (2011), earliest rifting in the Labrador Sea occurred in the Early Cretaceous (earliest Valanginian) and was accompanied by extrusion of the Alexis volcanics. These volcanics gave way to the widespread syn-rift Bjarni Formation consisting of arkosic sands with interbedded shales deposited in fault-bounded grabens and half-grabens until the end of the Albian by which time the setting had evolved from non-marine to marine. An erosional unconformity at the top of the Bjarni Formation marks the transition from early rifting to late rifting which was more regionally focused further offshore and was characterized by the shales of the Markland Formation whose deposition in deeper water conditions continued through the onset of seafloor spreading. The top of the Markland Formation corresponds to an unconformity, possibly related to uplift from the passage of the proto-Icelandic hotspot to the north. The shale dominated Cartwright and subsequent Kenamu formations, separated by a highly reflective unconformity, were contemporaneous with seafloor spreading during the Palaeogene and the unconformity is attributed to the major change in seafloor spreading direction that occurred between magnetic chron 25 and chron 24. The top of the overlying Kenamu Formation is marked by an unconformity of unknown origin that may be related to a nearby Late Eocene meteor impact in Labrador. Finally, the Mokami shales followed by the Saglek sandstones dominate the post-seafloor spreading period on the Labrador Shelf.

A tectonostratigraphic chart for the southwestern Greenland margin is available from Sørensen (2006) and, despite sparser well and seismic constraints, compares well with the Labrador Shelf and

with the Cretaceous to early Tertiary evolution of the Jeanne d'Arc Basin to the south (Deptuck *et al.* 2003; Sinclair & Withjack 2008) in terms of the timing of unconformities and the lithologies represented (Dickie *et al.* 2011). One curious departure from observed similarities as described by Dickie *et al.* (2011) is the absence of a prominent base Tertiary unconformity on the Labrador margin while the unconformity is observed both on the Greenland margin and the Jeanne d'Arc basin of the Grand Banks. While the cause of the unconformity is postulated to be widespread uplift from the proto-Icelandic hotspot (Dickie *et al.* 2011), it is not clear why the Labrador margin would have been spared from this influence.

4 GRAVITY DATA

Free air gravity anomalies over the Labrador Sea were obtained from the DNSC08 gravity anomaly compilation from the National Space Institute of the Technical University of Denmark (Andersen *et al.* 2008). These satellite altimetry data are an updated and augmented version of an earlier compilation from Sandwell & Smith (1997) of the results from both the Geosat Geodetic Mission and the ERS 1 Geodetic Phase mission. This new compilation provides improved coverage for short spatial scales and for both polar and coastal regions. The data used in the inversions for this study are shown in Fig. 3(a).

The Labrador coast exhibits a large positive gravity shelf edge effect due to the presence of the large Saglek and Hopedale basins over highly thinned crust (Srivastava 1978). A much less pronounced shelf edge effect is observed on the Greenland margin where no significant sedimentary basins exist. Apart from the sedimentary basins with their pronounced gravity highs, the western half of the Labrador Sea has a mildly negative gravity anomaly (-20 to 10 mGals) while the Greenland side is more positive (10–30 mGals).

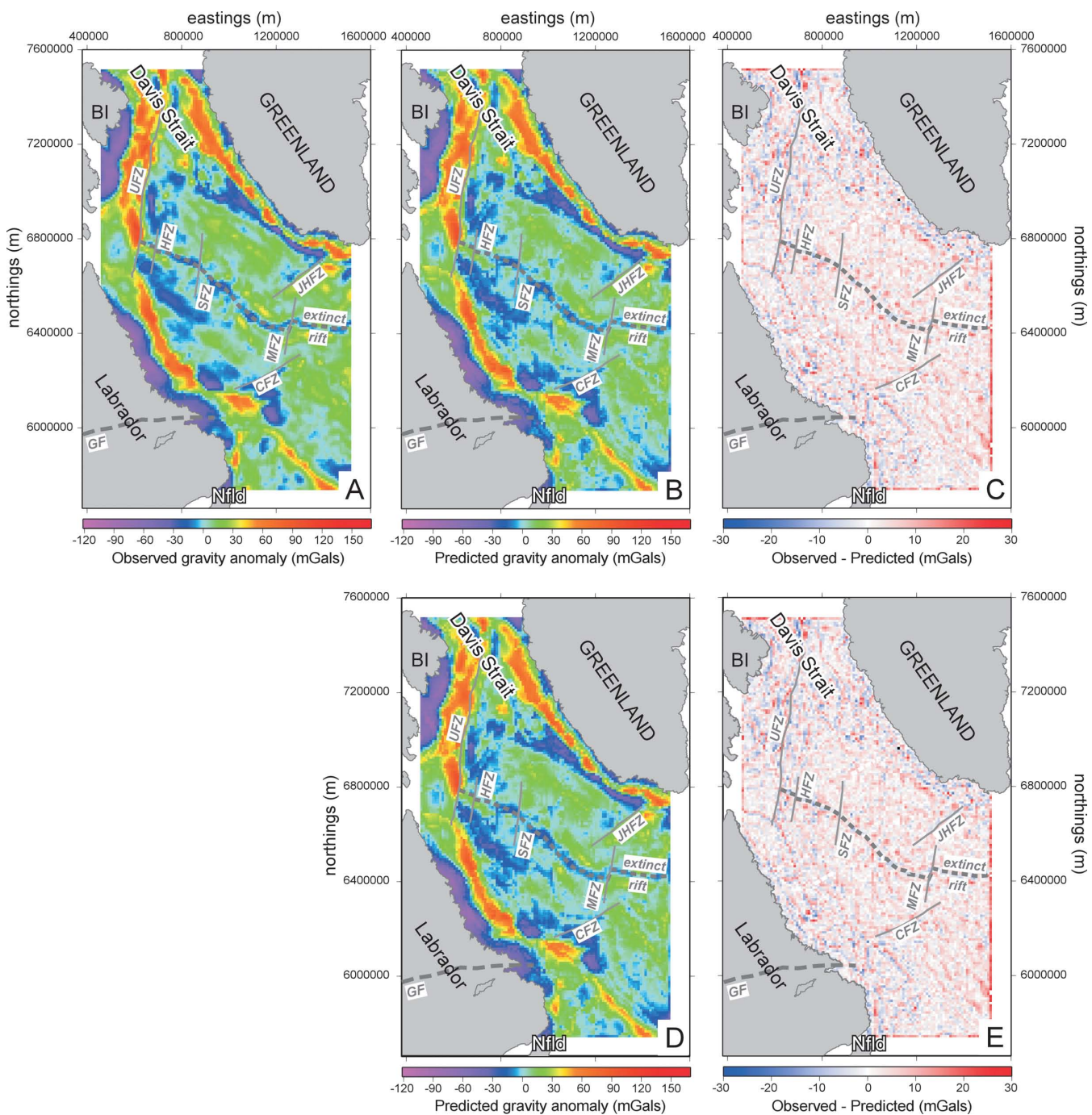


Figure 3. Maps of (a) observed free air gravity anomaly (averaged over 10 km for computational efficiency), predicted free air gravity anomaly map from the inverted density anomaly model derived using the NOAA constraints (b) and the GSC constraints (d), and (c) the difference between (a) and (b) and (e) the difference between (a) and (d). The white border in all panels corresponds to the area of padding cells used for the inversions. Note that both inversions generally fit the observations to within 10 mGals or less. The locations of the extinct rift (dashed grey line) and fracture zones (thin solid grey lines) within the Labrador Sea are plotted on all panels for reference. BI, Baffin Island; CFZ, Cartwright Fracture Zone; GF, Grenville Front; HFZ, Hudson Fracture Zone; JHFZ, Julian Haab Fracture Zone; MFZ, Minna Fracture Zone; Nfld, Newfoundland; SFZ, Snorri Fracture Zone; UFZ, Ungava Fault Zone.

At the centre of the Labrador Sea, gravity lows from a median rift at the ridge axis are offset by the main fracture zones (Srivastava 1978).

5 3-D GRAVITY INVERSION

The inversion methodology used for this study follows directly from earlier 3-D gravity inversion studies of the Newfoundland,

Irish Atlantic and Nova Scotian margins (Welford & Hall 2007; Welford *et al.* 2010; Dehler & Welford 2012; Welford *et al.* 2012). As in those studies, regional 3-D gravity inversion is used to provide large-scale depth to Moho, crustal density distribution and crustal thickness estimates over a broad area using only bathymetric and sediment thickness information to constrain the inverted results. Due to their sparseness, constraints from localized seismic studies are not used to constrain the inversion directly but are used indirectly

to decide on optimal inversion parameters such as mesh depth and reference density and to gauge the overall success of a particular inversion.

5.1 Inversion methodology

The GRAV3D inversion algorithm, developed by Li & Oldenburg (1996, 1998), is used to invert gravity observations at the Earth's surface and generate a subsurface 3-D density anomaly model (relative to an arbitrary reference density) that can reproduce those observations (within the data error bounds). During the inversion, the anomalous mass required to reproduce a given gravity anomaly is vertically distributed within the underlying model with that distribution fundamentally controlled by a depth-weighting function but also according to assigned smoothing parameters and also relative to a reference density model if one is used. For this study, a reference density anomaly model constrained by bathymetric and sediment thickness information was used, essentially forcing the inversion to distribute any remaining anomalous mass at depth beneath these two shallower prescribed layers.

One of the measures of success for any inversion is the misfit which corresponds to how closely the gravity predictions computed from the model fit the observations in a least-squares sense given the errors associated with those observations. The difference between the observed and predicted gravity values is further weighted by the reciprocal of the observed data errors such that the target misfit for the inversion is dimensionless and should be equal to the number of data points provided that the data errors are independent and Gaussian with zero mean (Li & Oldenburg 1998).

With the GRAV3D algorithm, a specific starting density anomaly relative to a prescribed reference density is assigned to each cell within the reference density anomaly model along with bounds over which that density anomaly is allowed to vary during the inversion to satisfy the observations. The bounds can be made tighter for well constrained portions of the reference model such as the water column. GRAV3D uses a mesh consisting of rectangular prisms of arbitrary size. For this study, the mesh was constructed from flattened cubes with lateral dimensions of $5\text{ km} \times 5\text{ km}$ and 500 m thick. The horizontal extent of the mesh corresponded to the study area shown in Fig. 1 and contained 244 cells in the eastings direction and 388 cells in the northings direction.

As stated, the vertical distribution of anomalous mass in the computed density anomaly model is fundamentally controlled by a depth-weighting function, by the assigned vertical smoothing parameter and by the use of a reference model. As demonstrated in Welford & Hall (2007) and Welford *et al.* (2010), the choice of mesh depth and reference density are also critical and interdependent. For a reference density of 2670 kg m^{-3} , the best match between seismic Moho obtained from other studies and an isodensity Moho-proxy from the gravity inversion was obtained for a mesh that was 25 km deep (Welford & Hall 2007). For a higher density of 2850 kg m^{-3} , the best match was obtained for a mesh that was 35 km deep (Welford *et al.* 2010). For this study, a deeper mesh of 40 km was sought to encompass the thicker unstretched crust of the margins of the Labrador Sea and the best match with the seismic Moho was obtained for a reference density of 2950 kg m^{-3} . This interplay between mesh depth and reference density makes intuitive sense since the anomalous mass required to reproduce a given gravity anomaly does not change but will be spread over fewer or more cells depending on the total depth of the mesh used. In other words, a specific gravity anomaly will be reproduced by a specific density

anomaly. A higher reference density will result in more mesh cells having a negative density anomaly and so more mesh cells with positive density anomalies will be required at depth to generate the same gravity anomaly as would be obtained with a lower reference density and a shorter mesh.

The free air gravity data used in the Labrador Sea inversion are shown in Fig. 3(a). The gravity point measurements were averaged over a $10\text{ km} \times 10\text{ km}$ grid in order to reduce the number of observations used in the inversion and consequently to significantly reduce the computation time and memory requirements. A 65-km -wide band of padding cells was placed around the study area. Errors for individual gravity data point measurements were not available but the overall accuracy of the gravity anomalies was reported as ranging from 4 to 7 mGals based on comparisons with ship track data (Sandwell & Smith 1997). As such, an error of 5 mGals was arbitrarily chosen for each of the averaged measurements. Picking a lower error would result in a more structured model for a given misfit value.

For the Labrador Sea inversions, a 3-D density anomaly model was generated that was smooth over length scales of 25 km in the eastings and northings directions and smooth over a length scale of 5 km in depth. A relaxed target misfit of two times the number of averaged data points was chosen in order to reproduce the long wavelength gravity anomalies using a coarse mesh. Lower misfits produced less geologically reasonable (i.e. introduced high frequency structure) density anomaly models that bore less resemblance to models from complementary geophysical methods.

5.2 Constraints

Bathymetric constraints for the Labrador Sea were obtained from the General Bathymetric Chart of the Oceans (GEBCO) global 30-arcsec -gridded bathymetric data set (http://www.gebco.net/data_and_products/gridded_bathymetry_data). This data set, generated primarily from quality-controlled ship depth soundings and contributions from the International Bathymetric Chart of the Arctic Ocean (IBCAO), is an interpolated data set with the interpolation guided by satellite altimetry bathymetry measurements which are not independent from the satellite gravity data used in the inversion. However, within the study area, 144 112 well distributed depth sounding measurements exist and these, combined with the IBCAO data, total 1 687 516 independent data points representing over 38 per cent of the bathymetric constraints used. Consequently, while the bathymetric constraints are not completely independent of the satellite gravity data, there is significant independent control on the bathymetric depths used. Plus, since the mesh used for the inversion is relatively coarse in depth (500 m deep cells) and provided the bathymetric depths are not off by kilometres, errors should have only a minor and localized impact on the inversion results. The bathymetric data for the Labrador Sea (Fig. 2a) were incorporated into the reference density anomaly model by forcing all model prisms above the bathymetric depths to contain density anomalies corresponding to ocean water (-1920 kg m^{-3} relative to a background density of 2950 kg m^{-3}). These density anomaly values were not allowed to vary during the inversion.

Depth to basement constraints were obtained from two sources and each set of constraints was used in a separate inversion in order to gauge the sensitivity of the inversion to the basement constraints and to investigate the non-uniqueness inherent to gravity inversion. The first constraints were minimum sediment

thickness estimates obtained from the National Geophysical Data Centre (NGDC) of the National Oceanic and Atmospheric Administration (NOAA) Satellite Information Service [(Divins 2003), <http://www.ngdc.noaa.gov/mgg/sedthick/>]. These were combined with the bathymetric constraints from Fig. 2(a) to obtain the depth to basement map of Fig. 2(b). The second depth to basement constraints were obtained from a compilation from the Geological Survey of Canada (Oakey & Stark 1995). Both sets of depth to basement/sediment thickness constraints were independently compiled from isopach maps, ocean drilling results and seismic reflection profiles. As such, there is a wide range of sources and vintages for both data sets and quantifying errors is difficult. Nonetheless, the coarseness of the mesh in depth (500 m deep cells) should only yield minor and localized anomalies on the inversion results unless the depth to basement errors extend over large regions and are on the order of kilometres.

Sediments were incorporated into the reference density model using the approach outlined in Welford *et al.* (2010) which evolved from examination of compaction curves with density as a function of depth for comparable sediments on the Nova Scotian margin (Albertz *et al.* 2010). In brief, a low starting density anomaly of -980 kg m^{-3} (corresponding to an absolute density of 1970 kg m^{-3}) was assigned to the top 2 km of the sedimentary basins and a starting density anomaly of -230 kg m^{-3} (corresponding to an absolute density of 2720 kg m^{-3}) was assigned for deeper parts of the basins and below. While the density anomaly values within the shallow sedimentary prisms were then allowed to vary between -1280 and -680 kg m^{-3} , corresponding to densities of 1670 – 2270 kg m^{-3} , the allowable density ranges for deeper parts of the basins were made depth dependent so as not to impose a hard boundary at the base of the sedimentary succession. This approach also limited the negative impact of inadvertently using erroneous sediment thickness estimates in the inversion. During the inversion, the density anomaly in each of the prisms beneath the sedimentary basins was allowed to vary between -510 and 420 kg m^{-3} (corresponding to a range in densities of 2440 – 3370 kg m^{-3}). Thus, the reference density anomaly model was completely homogeneous beneath the sediments (i.e. no layering) and the inversion was given great flexibility in assigning density anomalies beneath the sediments to reproduce the observed gravity response and no constraints were placed on which prisms should correspond to crustal rocks (with density anomalies of approximately less than 70 kg m^{-3} , absolute density of 3020 kg m^{-3}) and which prisms should correspond to upper mantle rocks (with density anomalies of approximately greater than 70 kg m^{-3} , absolute density of 3020 kg m^{-3}).

5.3 Corroborating evidence

Wide-angle seismic reflection/refraction models provide the best independent means against which to gauge the local reliability of the inverted results, bearing in mind that the seismic results were used to guide the choice of the maximum depth of the inverted mesh. The seismic constraints are not incorporated directly into the inversion due to their sparse coverage, due to uncertainties in the correspondence between seismic velocities and densities and because the inverted results are meant to provide an independent yet complementary view of the study area.

Crustal-scale studies have been undertaken in the Labrador Sea by the Geological Survey of Canada (GSC) and as part of the Lithoprobe Eastern Canadian Shield Onshore-Offshore Transect (ECSOOT; Hall *et al.* 2002). The GSC studies were focused on

investigating the Labrador Sea from one margin across to the other (Keen *et al.* 1994; Chian *et al.* 1995b; Reid 1996) while the Lithoprobe studies were focused solely on the Labrador margin (Funck & Louden 1998, 1999, 2000; Funck *et al.* 2001a,b, 2008). Studies of the Greenland margin have been fewer (Chian & Louden 1992; Gohl & Smithson 1993; Chian & Louden 1994; Funck *et al.* 2007) but have revealed the presence of an 80-km-wide transition zone underlain by serpentized mantle in the south (Chian & Louden 1994; Chian *et al.* 1995a) and underplated crust in the north (Gohl & Smithson 1993). A similar transition zone has been interpreted for the central Labrador margin (Chian *et al.* 1995b). The central rift of the Labrador Sea has also been investigated in detail revealing anomalously thin oceanic crust in the south (Osler & Louden 1992, 1995) and evidence for magmatic addition in the north (Funck *et al.* 2007; Gerlings *et al.* 2009).

From a deep seismic perspective, there are two complete composite profiles that cross the Labrador Sea. The first is in the central non-volcanic/magma-poor part (901, 902 and 903; Keen *et al.* 1994; Srivastava & Keen 1995) while the second is at the northern limit of the Labrador Sea in the Davis Strait (NUGGET line N1; Funck *et al.* 2007) where plume related volcanism is observed.

Most recently, Keen *et al.* (2012) have reinterpreted vintage seismic reflection data and have identified evidence of volcanic rifted basement in the northern Labrador Sea, extending 500 km to the south of earlier interpretations. The magmatic event that produced the interpreted volcanic features is believed to have followed an earlier period of non-volcanic rifting.

5.4 Inversion results

By inverting for the averaged free air gravity data using the reference density anomaly models and the parameters outlined above, 3-D density anomaly models were generated that were able to successfully reproduce the gravity observations over the Labrador Sea both in magnitude and in spatial distribution (Figs 3b and d). Subtle striping of the predicted data is a result of computer memory limitations on the imposed error threshold on reconstructing the compressed sensitivity matrix for the inversions. However, this striping does not impact the broader, long wavelength results which are the focus of this study. The difference plots between the observed and predicted data (Figs 3c and e) show a consistent fit throughout the study area with most differences less than 15 mGals.

The 3-D density anomaly distributions resulting from the constrained inversions are analysed in several ways. First, a density anomaly isosurface within each volume is chosen as a Moho-proxy (Figs 4a and b) and this boundary is compared with constraints from wide-angle reflection/refraction profiling (WARRP) results along slices through the volume that correspond with those surveys (Figs 5–7). Combining the depth to basement constraints (Figs 2b and c) with the inferred Moho-proxies (Figs 4a and b), crustal basement thickness was derived and used to obtain estimates of crustal extension, β , across the Labrador Sea (Fig. 8). The crustal basement is further subdivided according to density anomaly values into upper, middle and lower crust to better gauge depth-dependent extension (Fig. 9).

5.4.1 Moho variations

The Moho is a seismic discontinuity that marks the abrupt or gradational boundary between the crust and mantle. Typically, the Moho

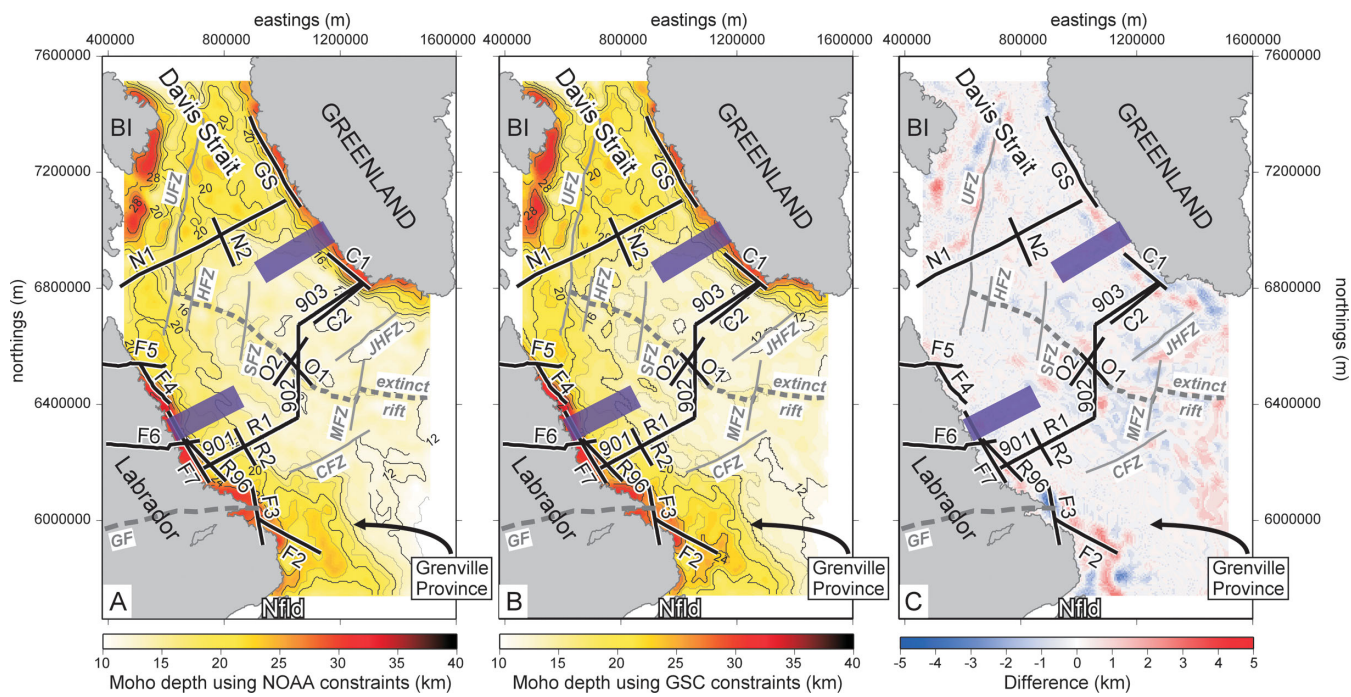


Figure 4. Moho depth (proxy) based on the 70 kg m^{-3} isosurface in the density anomaly model (corresponding to a density isosurface of 3020 kg m^{-3}) for the inversions using the NOAA constraints (a) and the GSC constraints (b). The difference between the two plots is shown in (c) where it is evident that both inversions generally agree to within 2 km. Key published deep seismic lines against which the Moho-proxy results can be compared are plotted with the solid black lines, see text for line label references. The locations of the extinct rift (dashed grey line) and fracture zones (thin solid grey lines) within the Labrador Sea are plotted for reference. The purple boxes show the location of the non-volcanic to volcanic transition on both margins proposed by Keen *et al.* (2012). BI, Baffin Island; CFZ, Cartwright Fracture Zone; GF, Grenville Front; HFZ, Hudson Fracture Zone; JHFZ, Julian Haab Fracture Zone; MFZ, Minna Fracture Zone; Nfld, Newfoundland; SFZ, Snorri Fracture Zone; UFZ, Ungava Fault Zone.

boundary corresponds to seismic P-wave velocities that are greater than 7.9 km s^{-1} and its location and structure is determined using wide-angle reflection/refraction profiling (WARRP). While the Moho does not correspond with a specific density contrast, a Moho-proxy can be defined if it is assumed that subbasin mass variations are caused by Moho variations and not from internal mass variations within the crust and/or mantle. For this study, the Moho-proxy was chosen to correspond with the 70 kg m^{-3} isosurface (3020 kg m^{-3} relative to a reference density of 2950 kg m^{-3}) as this Moho-proxy showed the best and most consistent match with available seismic constraints of Moho depth.

The Moho-proxy maps using the two sets of depth to basement constraints (Figs 4a and b) show a relatively uniform Moho depth of 12 km in the centre of the Labrador Sea with a deeper Moho (20 km and greater) beneath the Davis Strait and for the offshore extension of the Grenville Province of southeastern Labrador. Along both the Labrador and Greenland margins, an abrupt shallowing of the Moho is observed immediately offshore with significant along-strike variations in the distribution of the deeper Moho along the margins. There does not appear to be a change in Moho character or depth across the non-volcanic to volcanic transition zone interpreted by Keen *et al.* (2012).

Slices through the northern Labrador Sea (Fig. 5) show an excellent correspondence between the Moho-proxies and the seismically derived Moho along the NUGGET lines [N1 (Funck *et al.* 2007) and N2 (Gerlings *et al.* 2009)]. While a significant discrepancy exists between the Moho-proxy and the seismic Moho modelled offshore Greenland in the Davis Strait (GS; Gohl & Smithson 1993), there is excellent correspondence between the Moho-proxy and the top of a high velocity zone modelled by Gohl & Smithson (1993) demon-

strating that the Moho-proxy may underestimate the depth to the seismic Moho in areas where a lower crustal high velocity zone or underplate exists.

Through the middle of the Labrador Sea (Fig. 6), seismic reflection profiles were used to guide forward gravity modelling of the crust and upper mantle along profiles 901 and 903 (Keen *et al.* 1994) and the resulting Moho generally matches well with the Moho-proxies from this study. An even better fit is obtained with Moho constraints from WARRP studies along profiles C2 (Chian & Louden 1994), O2 (Osler & Louden 1992, 1995), R1 and R2 (Chian *et al.* 1995b). Along strike of the Greenland shelf, the WARRP results slightly overestimate the depth to Moho compared to the Moho-proxies along profile C1 (Chian & Louden 1992).

Along the Labrador Shelf, numerous WARRP profiles exist from the Lithoprobe project [F2 and F3 (Funck *et al.* 2001b), F4 (Funck & Louden 1998), F5 (Funck & Louden 1999), F6 (Funck & Louden 2000), F7 (Funck *et al.* 2008)] and from the GSC (R96; Reid 1996). In general, the seismically derived Moho from these lines agrees well with the inverted Moho-proxies with an average Moho depth of 25–30 km (Fig. 7). The main exception is profile F2 where the seismically modelled Moho is significantly deeper (15–20 km or more) than the Moho-proxies which lie between 20 and 25 km depth. Similar to the results along profile GS (Fig. 5), results from modelling of WARRP data along profile F2 have revealed a high velocity zone (Funck *et al.* 2001b), the top of which lies closer to the Moho-proxy but still 5–10 km deeper. This localized high velocity lower crustal feature likely represents an underplate and the lower crust may have been altered during its emplacement leading to higher than average lower crustal densities.

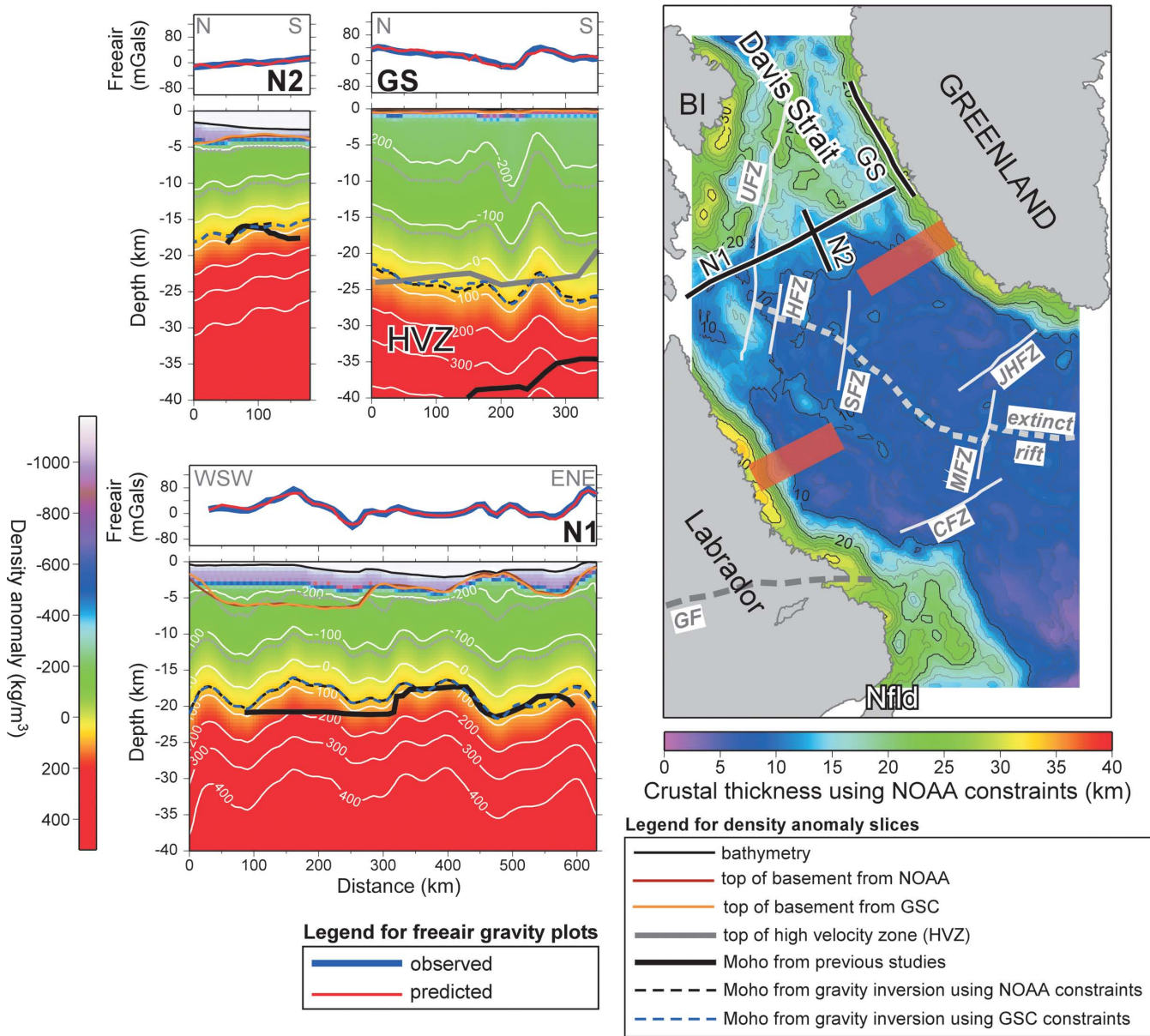


Figure 5. Slices through the inverted density anomaly model from the inversion using the NOAA constraints along seismic lines that sample the northern limit of the Labrador Sea and into Davis Strait. A comparison between the observed free air gravity anomalies (blue line) and the anomalies predicted for the inverted density anomaly model (red line) is plotted above each slice. The overlain thick black lines on the density anomaly slices correspond to the Moho depths obtained from previous studies and the dashed black lines are from the gravity inversion using the NOAA constraints. For comparison, the equivalent Moho-proxy obtained from the inversion using the GSC constraints is shown with the blue dashed line which generally matches the NOAA inversion results. On the GS slice, the grey thick line shows the top of a high velocity zone modelled by Gohl & Smithson (1993). Labelled line locations are plotted on a map of crustal thickness derived from the depth to basement (Fig. 2b) and the Moho-proxy (Fig. 4) from the inversion using the NOAA constraints. On the map, the locations of the extinct rift (dashed grey line) and fracture zones (thin solid grey lines) within the Labrador Sea are plotted for reference. The orange boxes on the map show the location of the non-volcanic to volcanic transition on both margins proposed by Keen *et al.* (2012). BI, Baffin Island; CFZ, Cartwright Fracture Zone; GF, Grenville Front; HFZ, Hudson Fracture Zone; JHFZ, Julian Haab Fracture Zone; MFZ, Minna Fracture Zone; Nfld, Newfoundland; SFZ, Snorri Fracture Zone; UFZ, Ungava Fault Zone.

5.4.2 Variations in crustal extension

The depth to basement constraints (Figs 2b and c) are combined with the inverted Moho-proxy depth models (Figs 4a and b) to compute crustal basement thickness across the Labrador Sea. The resulting crustal thicknesses for the inversion using the NOAA constraints are plotted in Fig. 8(a). This map reveals that most of the Labrador Sea is underlain by 5- to 10-km-thick crust while the crustal basement in the Davis Strait is at least 20 km thick, consistent with previous

studies (Louden *et al.* 2004). Crustal basement thickness along the Labrador and Greenland continental shelves increases from 20 to 30 km landward with significant along strike variations. It should be stressed that the crustal thickness is underestimated on this map in regions where an anomalously high density lower crust or an underplate exists, such as offshore southeastern Labrador beneath the seaward extension of the Grenville province.

Estimates of unstretched crustal thickness for Labrador vary greatly from as little as 30 km for the Makkovik Block to as much

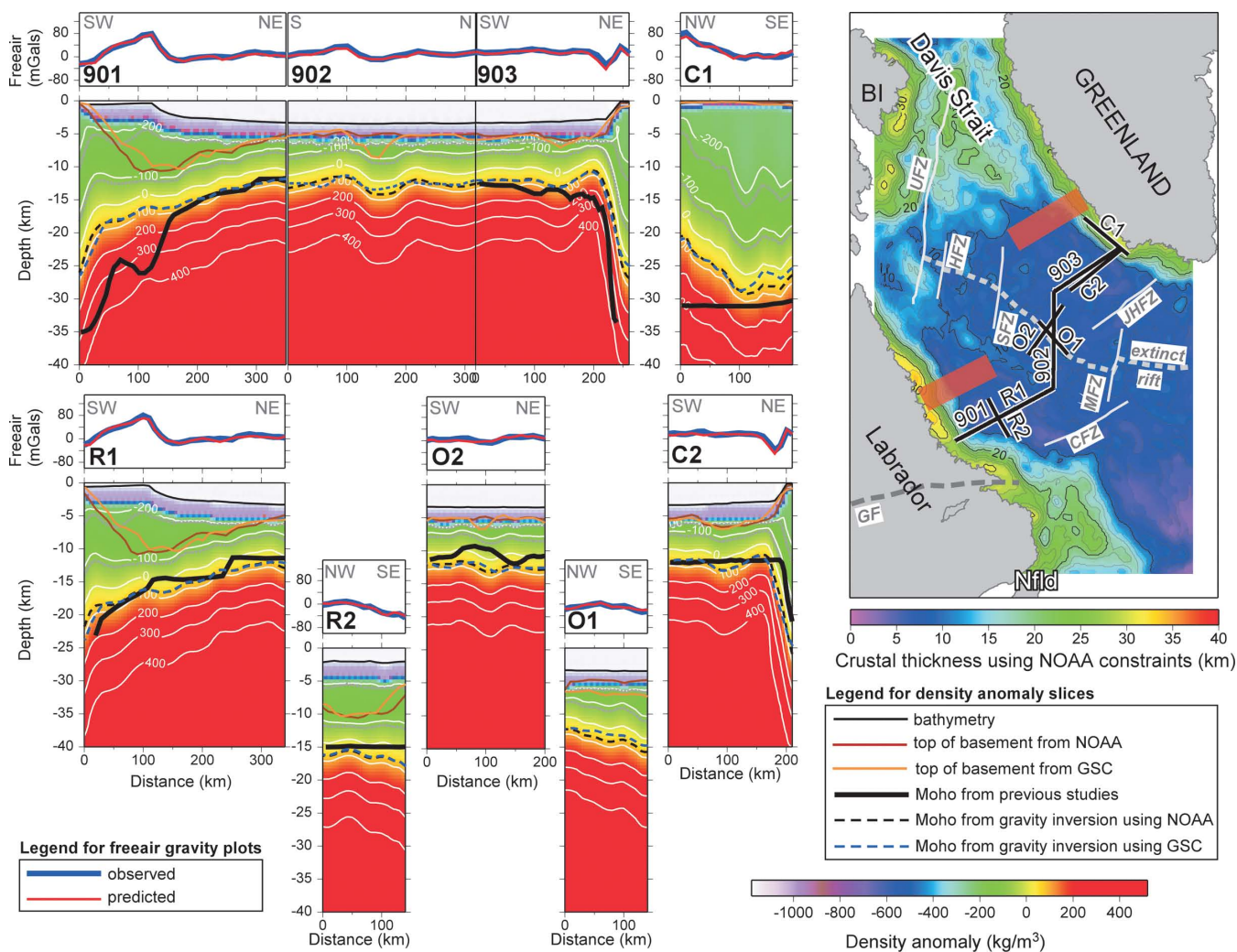


Figure 6. Slices through the inverted density anomaly model from the inversion using the NOAA constraints along seismic lines that cut across the centre of the Labrador Sea. A comparison between the observed free air gravity anomalies (blue line) and the anomalies predicted for the inverted density anomaly model (red line) is plotted above each slice. The overlain thick black lines on the density anomaly slices correspond to the Moho depths obtained from previous studies and the dashed black lines are from the gravity inversion using the NOAA constraints. For comparison, the equivalent Moho-proxy obtained from the inversion using the GSC constraints is shown with the blue dashed line which generally matches the NOAA inversion results. Labelled line locations are plotted on a map of crustal thickness derived from the depth to basement (Fig. 2b) and the Moho-proxy (Fig. 4) from the inversion using the NOAA constraints. On the map, the locations of the extinct rift (dashed grey line) and fracture zones (thin solid grey lines) within the Labrador Sea are plotted for reference. The orange boxes on the map show the location of the non-volcanic to volcanic transition on both margins proposed by Keen *et al.* (2012). BI, Baffin Island; CFZ, Cartwright Fracture Zone; GF, Grenville Front; HFZ, Hudson Fracture Zone; JHFZ, Julian Haab Fracture Zone; MFZ, Minna Fracture Zone; Nfld, Newfoundland; SFZ, Snorri Fracture Zone; UFZ, Ungava Fault Zone.

as 50 km for the Grenville Province (Funck & Louden 1999, 2000; Funck *et al.* 2001b; Hall *et al.* 2002). For Greenland, there are fewer controlled source seismic constraints on crustal thickness but some estimates are available from teleseismic studies (Dahl-Jensen *et al.* 2003). In Fig. 8(d), a model of variable unstretched crustal thickness was constructed by combining available onshore crustal thickness constraints (open circles) with extrapolated data points (white circles) that ensured the extension of thickness trends perpendicular to magnetic anomalies in the oceanic domain and along orogenic trends such as the Grenville front on land. Using both a uniform unstretched crustal thickness of 35 km and the variable unstretched crustal thickness model in Fig. 8(d), the crustal thickness in Fig. 8(a) was plotted as a percentage of the unstretched crust (Figs 8b and e). These maps reveal that most of the deep crust beneath the Labrador Sea has been thinned by 70–90 per cent while the shelves have been thinned significantly less.

The crustal basement thickness information is reposed in terms of estimates of the extension/stretching factor, β , across the Labrador Sea in Figs 8(c) and (f). These β value maps are replotted in Fig. 9 where they are overlain with the oceanic and transitional zones interpreted by Chalmers & Pulvertaft (2001) and Gerlings *et al.* (2009). The extension factors, which correspond to the ratio of extended length to unextended length, were computed by assuming 2-D extension and by taking a 1-km-long block of unextended crust (35 km or variable model) and computing the extended length for the varying crustal thicknesses in the study region by assuming that the cross-sectional area remains constant. Two contours are highlighted in the extension factor maps (Figs 8c, f and 9), the white solid $\beta = 2$ contour which corresponds to the stretching factor above which polyphase faulting becomes important (Reston 2007) and the white dashed $\beta = 3.5$ contour which corresponds to the stretching factor above which embrittlement of the entire crust is thought to

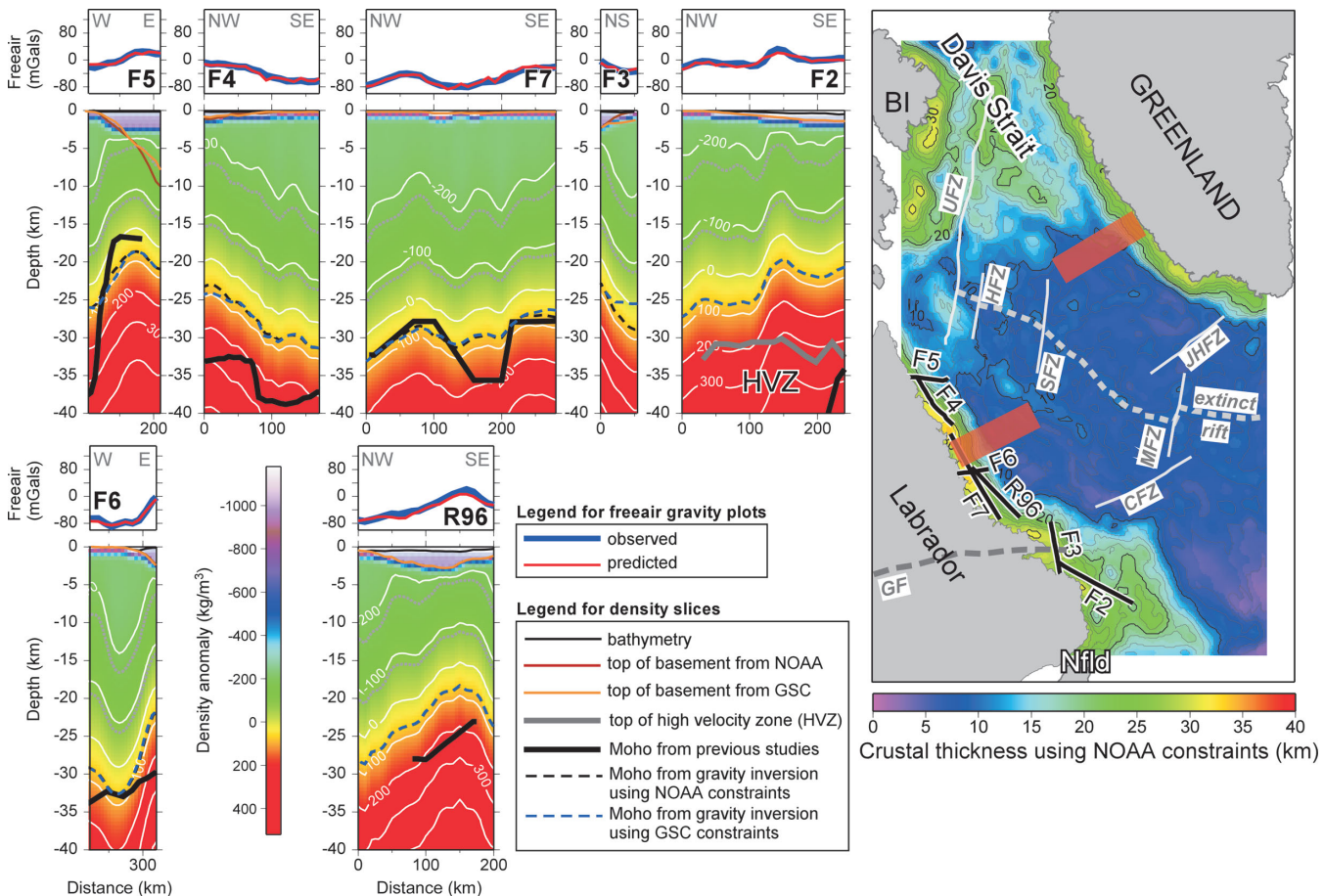


Figure 7. Slices through the inverted density anomaly model from the inversion using the NOAA constraints along seismic lines that sample the crust adjacent to the Labrador margin. A comparison between the observed free air gravity anomalies (blue line) and the anomalies predicted for the inverted density anomaly model (red line) is plotted above each slice. The overlain thick black lines on the density anomaly slices correspond to the Moho depths obtained from previous studies and the dashed black lines are from the gravity inversion using the NOAA constraints. For comparison, the equivalent Moho-proxy obtained from the inversion using the GSC constraints is shown with the blue dashed line which generally matches the NOAA inversion results. Labelled line locations are plotted on a map of crustal thickness derived from the depth to basement (Fig. 2b) and the Moho-proxy (Fig. 4) from the inversion using the NOAA constraints. On the map, the locations of the extinct rift (dashed grey line) and fracture zones (thin solid grey lines) within the Labrador Sea are plotted for reference. The orange boxes on the map show the location of the non-volcanic to volcanic transition on both margins proposed by Keen *et al.* (2012). BI, Baffin Island; CFZ, Cartwright Fracture Zone; GF, Grenville Front; HFZ, Hudson Fracture Zone; JHFZ, Julian Haab Fracture Zone; MFZ, Minna Fracture Zone; Nfld, Newfoundland; SFZ, Snorri Fracture Zone; UFZ, Ungava Fault Zone.

be possible based on numerical modelling studies (Pérez-Gussinyé & Reston 2001; Pérez-Gussinyé *et al.* 2003). Serpentization of the upper mantle can occur once total crustal embrittlement has occurred so the $\beta = 3.5$ contour can be viewed as a proxy for the landward limit of potential serpentization.

The choice of the uniform 35-km-thick unstretched crustal model versus the variable unstretched crustal thickness model (Fig. 8d) did not significantly alter the location of the two contours in Figs 8(c) and (f) other than for the offshore extension of the Grenville province where the variable model shows polyphase faulting to be important, although this likely only reflects that the lower crust is of anomalously high density in this region and the Moho-proxy should be deeper. This also appears to be the case to a lesser extent for the Davis Strait although the constraints for the variable thickness model are sparser (Fig. 8d). The location of the $\beta = 3.5$ contour does not vary significantly between Figs 8(c) and (f) although overall β values oceanward of this contour are larger due to the thicker crust in the variable thickness model.

The northern limit of the zone of possible serpentization in Figs 8(c), (d) and 9 roughly corresponds with the non-volcanic to

volcanic transition zone proposed by Keen *et al.* (2012), certainly on the Greenland margin, and there is good correspondence between this zone and the interpreted serpentinites and southern transitional crust from Chalmers & Pulvertaft (2001) and Gerlings *et al.* (2009). These maps suggest that a broad zone of serpentization likely exists beneath all of the Hopedale Basin and beneath the southern half of the Saglek Basin on the Labrador margin, regions where serpentized mantle has previously been interpreted (Chian *et al.* 1995b; Keen *et al.* 2012).

5.4.3 Evidence for depth-dependent stretching

The region of inferred crustal basement within the inverted 3-D density anomaly volumes can be extracted and subdivided to allow for variations in the thickness of individual crustal layers to be investigated (Fig. 10). These subdivisions, which are delineated by the dashed grey lines on the slices in Figs 5–7, are intended to simplify description of the crustal density variations and aid in their interpretation. The upper crust is defined as corresponding to density anomaly values of less than -180 kg m^{-3} (absolute density

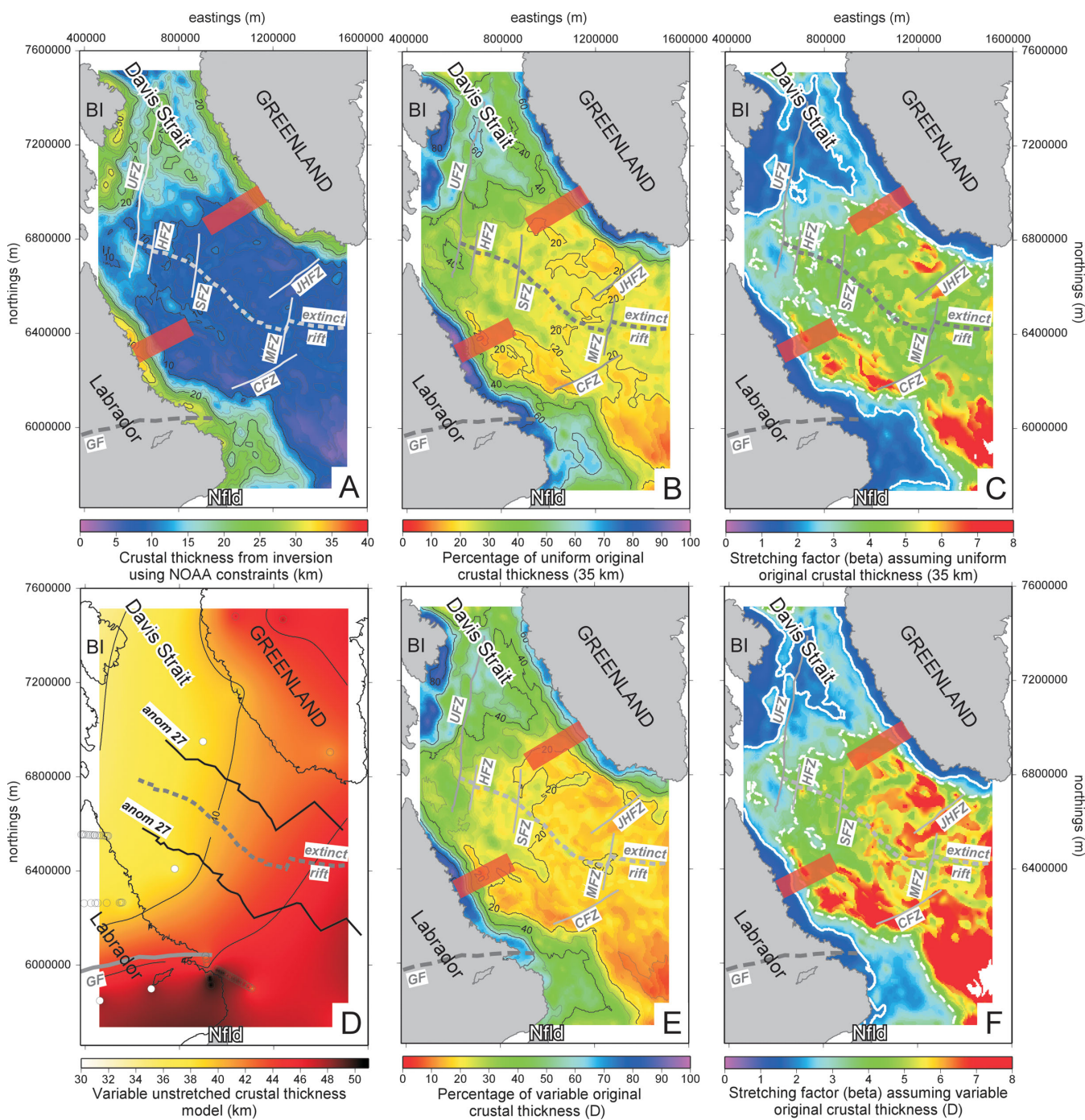


Figure 8. Map of project area showing (a) crustal thickness derived from the NOAA depth to basement constraints (Fig. 2b) and the inverted Moho-proxy (Fig. 4a) from the inversion using the NOAA constraints. Assuming a uniform original crustal thickness of 35 km, maps of crustal thickness as a percentage of original unstretched crust and of stretching factor, β , are presented in plots (b) and (c), respectively. A variable unstretched crustal thickness model for the Labrador Sea was constructed and extrapolated from controlled source and passive seismic constraints (Funck & Louden 1999, 2000; Funck *et al.* 2001b; Dahl-Jensen *et al.* 2003) and is plotted in (d). Maps of crustal thickness as a percentage of the variably thick original unstretched crust (d) and of the corresponding stretching factor, β , are presented in plots (e) and (f), respectively. On plots (c) and (f), the $\beta = 2$ contour, corresponding to the stretching factor above which polyphase faulting becomes important (Reston 2007), and the $\beta = 3.5$ contour, corresponding to the stretching factor above which embrittlement of the entire crust is possible (Pérez-Gussinyé & Reston 2001; Pérez-Gussinyé *et al.* 2003), are highlighted by the white solid and white dashed contour lines, respectively. Embrittlement of the entire crust can lead to serpentinization of the upper mantle and possible mantle exhumation. The locations of the extinct rift (dashed grey line) and fracture zones (thin solid grey lines) within the Labrador Sea are plotted on all panels for reference. The orange boxes on the maps show the location of the non-volcanic to volcanic transition on both margins proposed by Keen *et al.* (2012). BI, Baffin Island; CFZ, Cartwright Fracture Zone; GF, Grenville Front; HFZ, Hudson Fracture Zone; JHFZ, Julian Haab Fracture Zone; MFZ, Minna Fracture Zone; Nfld, Newfoundland; SFZ, Snorri Fracture Zone; UFZ, Ungava Fault Zone.

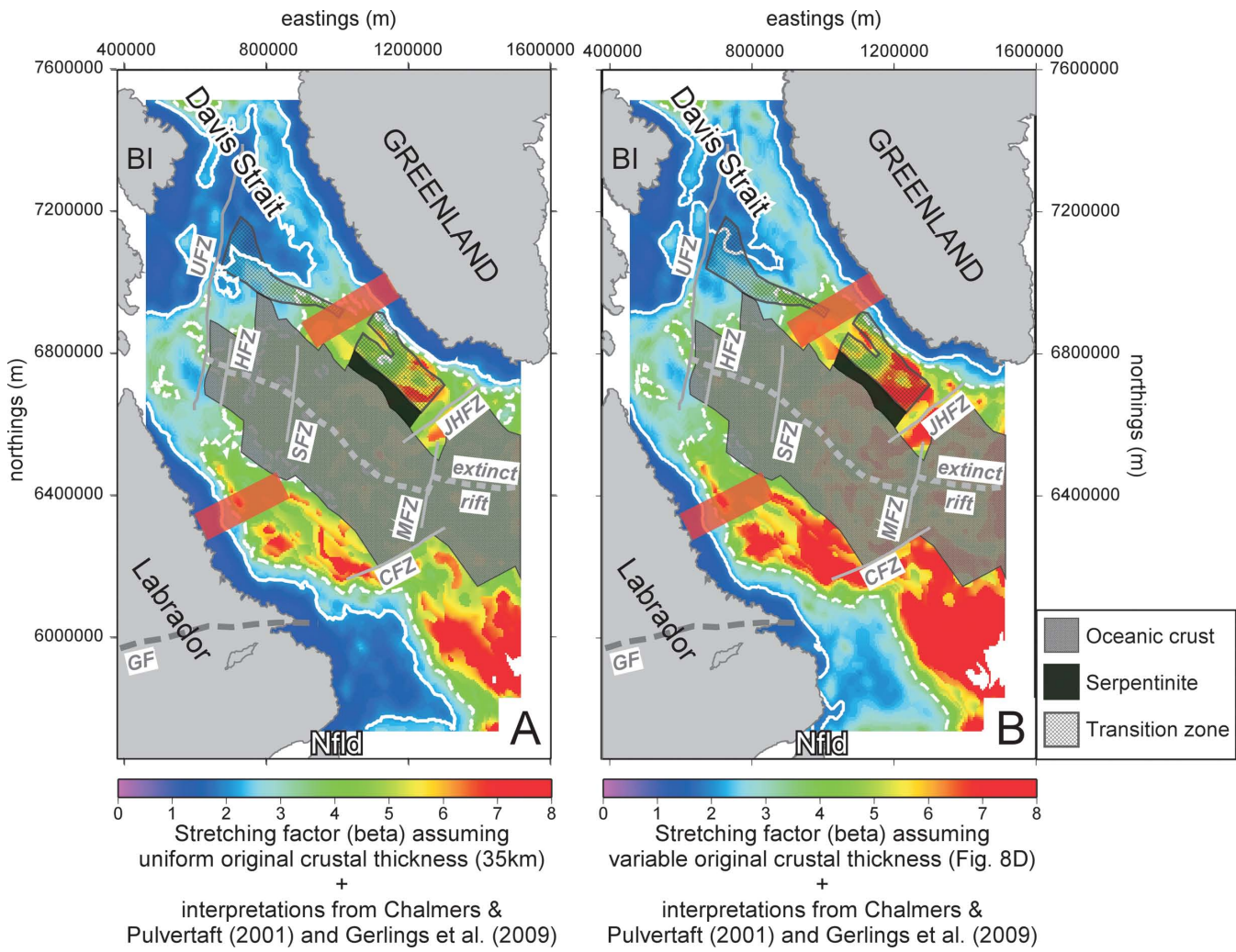


Figure 9. Maps of stretching factor, β , derived (a) using a uniform original crustal thickness of 35 km and (b) using a variable original crustal thickness model (Fig. 8d), with overlain oceanic and transitional crust interpretations from Chalmers & Pulvertaft (2001) and Gerlings *et al.* (2009). On both plots, the $\beta = 2$ contour, corresponding to the stretching factor above which polyphase faulting becomes important (Reston 2007), and the $\beta = 3.5$ contour, corresponding to the stretching factor above which embrittlement of the entire crust is possible (Pérez-Gussinyé & Reston 2001; Pérez-Gussinyé *et al.* 2003), are highlighted by the white solid and white dashed contour lines respectively. Embrittlement of the entire crust can lead to serpentization of the upper mantle and possible mantle exhumation. The locations of the extinct rift (dashed grey line) and fracture zones (thin solid grey lines) within the Labrador Sea are plotted on all panels for reference. The orange boxes on the maps show the location of the non-volcanic to volcanic transition on both margins proposed by Keen *et al.* (2012). BI, Baffin Island; CFZ, Cartwright Fracture Zone; GF, Grenville Front; HFZ, Hudson Fracture Zone; JHFZ, Julian Haab Fracture Zone; MFZ, Minna Fracture Zone; Nfld, Newfoundland; SFZ, Snorri Fracture Zone; UFZ, Ungava Fault Zone.

of 2770 kg m^{-3}), middle crust as corresponding to density anomaly values between -180 and -80 kg m^{-3} (between absolute densities of 2770 and 2850 kg m^{-3}) and lower crust as corresponding to density anomaly values between -80 and 70 kg m^{-3} (between absolute densities of 2850 and 3020 kg m^{-3}). The resulting upper, middle and lower crustal thicknesses are plotted as a percentage of the total crustal thickness in Figs 10(b)–(d), respectively. It is important to stress that in subdividing the crust according to layer properties commonly associated with continental crust, there is no distinction made between continental, transitional and oceanic crust in terms of physical properties and the assumption is also made that the rifting process itself does not significantly alter the physical properties of the rifted crust. These assumptions are problematic but as there is no unique and quantitative way of accounting for the physical property changes likely induced by rifting, hydration and eventual seafloor spreading such as compositional changes, density changes and the introduction of igneous material, the sim-

ple subdivision of the crustal layers on the basis of density is thought to be sufficient to capture gross crustal structural variations across the Labrador Sea. To aid in the interpretation of the results, the oceanic crust interpretation from Chalmers & Pulvertaft (2001) and Gerlings *et al.* (2009) is outlined in red on each plot of Fig. 10.

In Fig. 10(b), the inferred upper crustal densities make up less than 20 per cent of the crust in the centre of the Labrador Sea, which is expected for oceanic crust, but 30–50 per cent of the crust along the Labrador and Greenland shelf margins and into the Davis Strait. Surprisingly, a greater portion of upper crustal densities is observed within the zone of interpreted oceanic crust (outlined in red) compared to the transitional crustal zones to each side, outboard of the continental shelves. This may reflect extreme thinning of continental crust in the transitional zones and the preferential emplacement of exhumed serpentized mantle, much of which has yet to be resolved seismically.

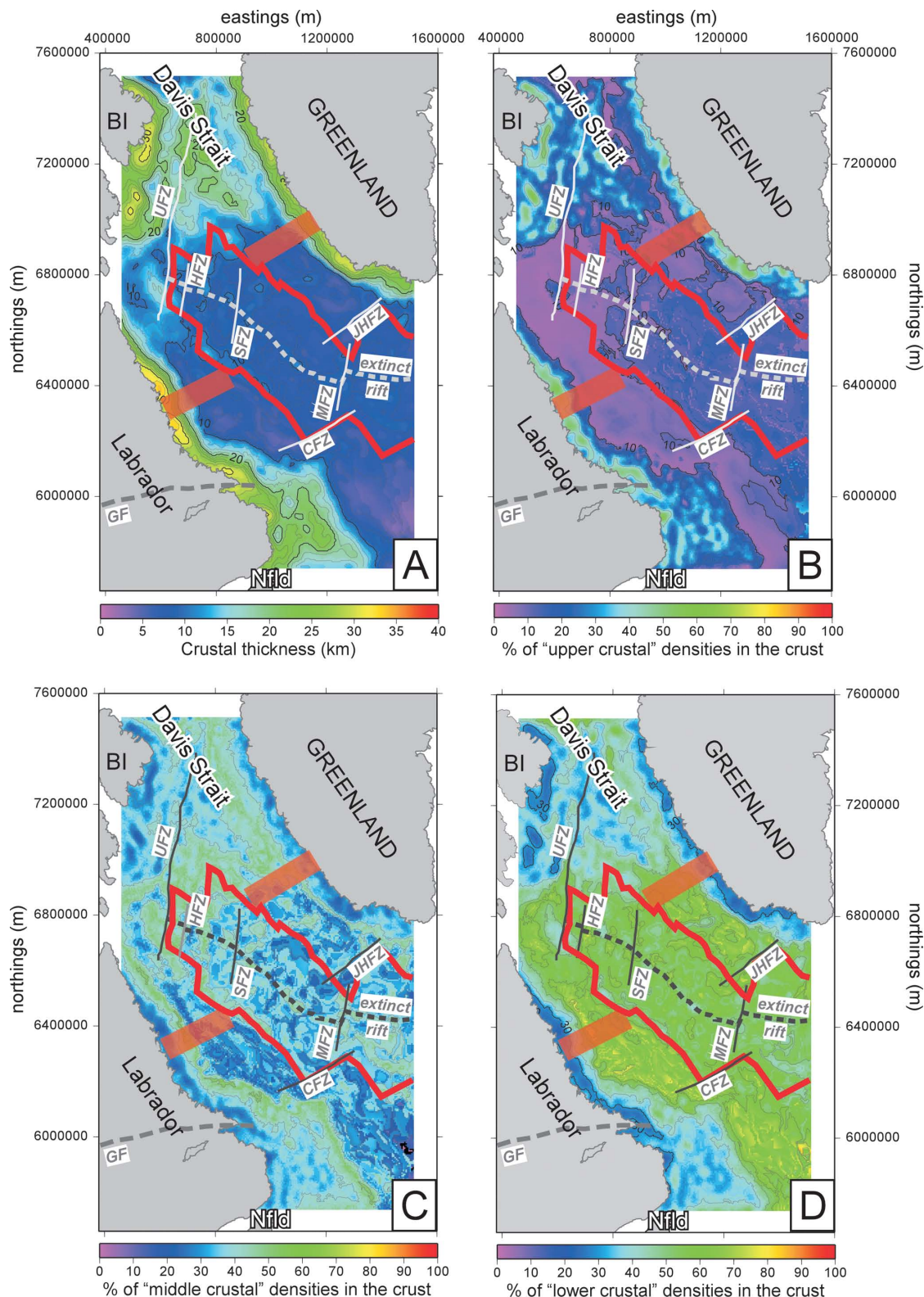


Figure 10. Maps of (a) crustal basement thickness computed from the NOAA depth to basement constraints (Fig. 2b) and the interpreted Moho depth surface (Fig. 4a) from the inversion using the NOAA constraints, (b) percentage of the total crustal basement thickness with density anomalies below 180 kg m^{-3} (i.e. upper-crustal-type densities, less than 2770 kg m^{-3}), (c) percentage of the total crustal basement thickness with density anomalies between -180 and -80 kg m^{-3} (i.e. middle-crustal-type densities, between 2770 and 2870 kg m^{-3}) and (d) percentage of the total crustal basement thickness with density anomalies between -80 and 70 kg m^{-3} (i.e. lower-crustal-type densities, between 2870 and 3020 kg m^{-3}). The oceanic crust interpretation from Chalmers & Pulvertaft (2001) and Gerlings *et al.* (2009) is outlined in red on each plot. The locations of the extinct rift (dashed grey line) and fracture zones (thin solid grey lines) within the Labrador Sea are plotted on all panels for reference. The orange boxes on the maps show the location of the non-volcanic to volcanic transition on both margins proposed by Keen *et al.* (2012). BI, Baffin Island; CFZ, Cartwright Fracture Zone; GF, Grenville Front; HFZ, Hudson Fracture Zone; JHFZ, Julian Haab Fracture Zone; MFZ, Minna Fracture Zone; Nfld, Newfoundland; SFZ, Snorri Fracture Zone; UFZ, Ungava Fault Zone.

Middle-crustal-type densities appear to be more uniformly distributed, making up 30–40 per cent of the crust, across the entire study area (Fig. 10c). A curious margin-parallel striped trend in the middle crustal density contributions is apparent on the Labrador margin although its cause is unclear.

Higher lower-crustal-type densities dominate over 50 per cent of the crust in the centre of the Labrador Sea but contribute much less to the continental shelves and in Davis Strait, although these estimates do not take into account the higher densities contributed by underplates or altered lower crust. Interestingly, lower crustal densities make up 5–10 per cent more of the transitional crustal zones relative to the oceanic crustal zone, perhaps highlighting zones where higher density serpentinized mantle has been exhumed.

6 DISCUSSION

6.1 Broad structure of the Labrador Sea

A fence diagram showing slices through the inverted 3-D density anomaly model from the inversion using the NOAA constraints both across and along the margins of the Labrador Sea is presented in Fig. 11. The location of the extinct rift as well as the location of the non-volcanic (in the south) to volcanic (in the north) transition zone proposed by Keen *et al.* (2012) are plotted relative to the slices.

Moho depth along the Labrador and Greenland shelves generally lies between 20 and 25 km depth with significant along strike variations that do not appear to correlate across the sea, partly due to the coarse picking of the slices. The slices that transect the Labrador Sea appear to display similar crustal characters with the main differences relating to the sharpness of the crustal necking at their landward ends, with the most abrupt necking observed on the Greenland margin, as has been observed in previous studies (Chian

et al. 1995b). The southernmost slice shows the widest and most gradual necking style on the Labrador margin but the contribution from the high velocity underplate modelled by Funck *et al.* (2001b) has not been included.

The non-volcanic to volcanic transition zone proposed by Keen *et al.* (2012) does not appear to correlate with any specific crustal thickness or density structure variations in Fig. 11. Consequently, this transition appears to be a much more subtle feature and influencing factor than the abrupt non-volcanic to volcanic transition observed on the Scotian margin (Dehler & Welford 2012), perhaps indicating that the transition in the Labrador Sea evolved temporally with the passage of the transient proto-Icelandic plume under Davis Strait rather than from a fundamental inherited lithospheric contrast at depth.

6.2 Sediment excess and deficiency in the Labrador Sea

The inferred crustal thickness from the inversion using the NOAA constraints (Fig. 8a) is compared with the NOAA sediment thickness estimates to assess sediment excess and deficiency in the Labrador Sea. Local Airy compensation is assumed as are constant densities for water (ρ_w), sediments (ρ_s), crust (ρ_c) and mantle (ρ_m). Sediment thickness (s) is found to be proportional to the amount of crustal thinning (dt) below the sediments such that

$$s = dt \frac{(\rho_m \rho_c)}{(\rho_m \rho_s)} W \frac{(\rho_m \rho_w)}{(\rho_m \rho_s)}. \quad (1)$$

Water depth (W) in the previous equation is obtained from the bathymetry and the crust is assumed to have been 35 km thick before thinning. Densities of 1030, 2200, 2850 and 3300 kg m⁻³ are assigned for ρ_w , ρ_s , ρ_c and ρ_m , respectively. Fig. 12 shows the deviations from the model of isostatically compensated sediment

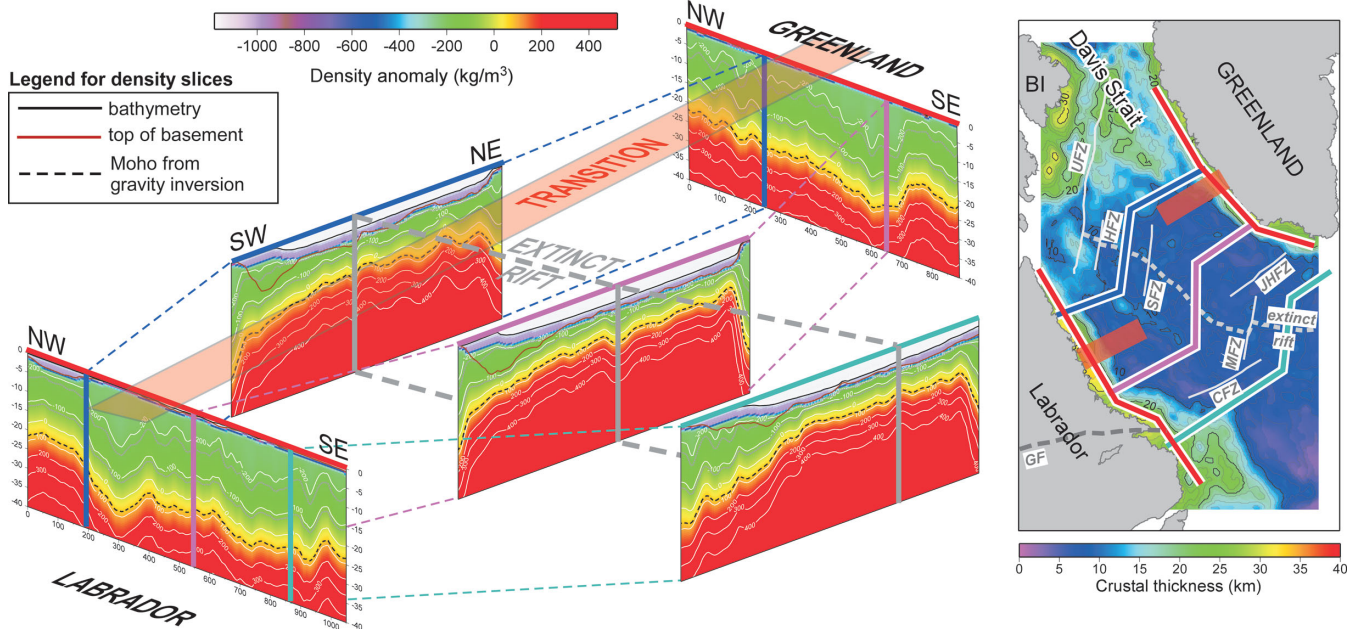


Figure 11. Fence diagram of arbitrary slices through the inverted density anomaly model from the inversion using the NOAA constraints with colour-coded slice locations overlain on a crustal basement thickness map derived from the NOAA depth to basement constraints (Fig. 2b) and the Moho-proxy (Fig. 4a) from the inversion using the NOAA constraints. The dashed black lines on each slice are the Moho-proxy depth from the gravity inversion. On the map, the locations of the extinct rift (dashed grey line) and fracture zones (thin solid grey lines) within the Labrador Sea are plotted for reference. The orange boxes on the map show the location of the non-volcanic to volcanic transition on both margins proposed by Keen *et al.* (2012) and this transition is also overlain on the fence diagram. BI, Baffin Island; CFZ, Cartwright Fracture Zone; GF, Grenville Front; HFZ, Hudson Fracture Zone; JHFZ, Julian Haab Fracture Zone; MFZ, Minna Fracture Zone; SFZ, Snorri Fracture Zone; UFZ, Ungava Fault Zone.

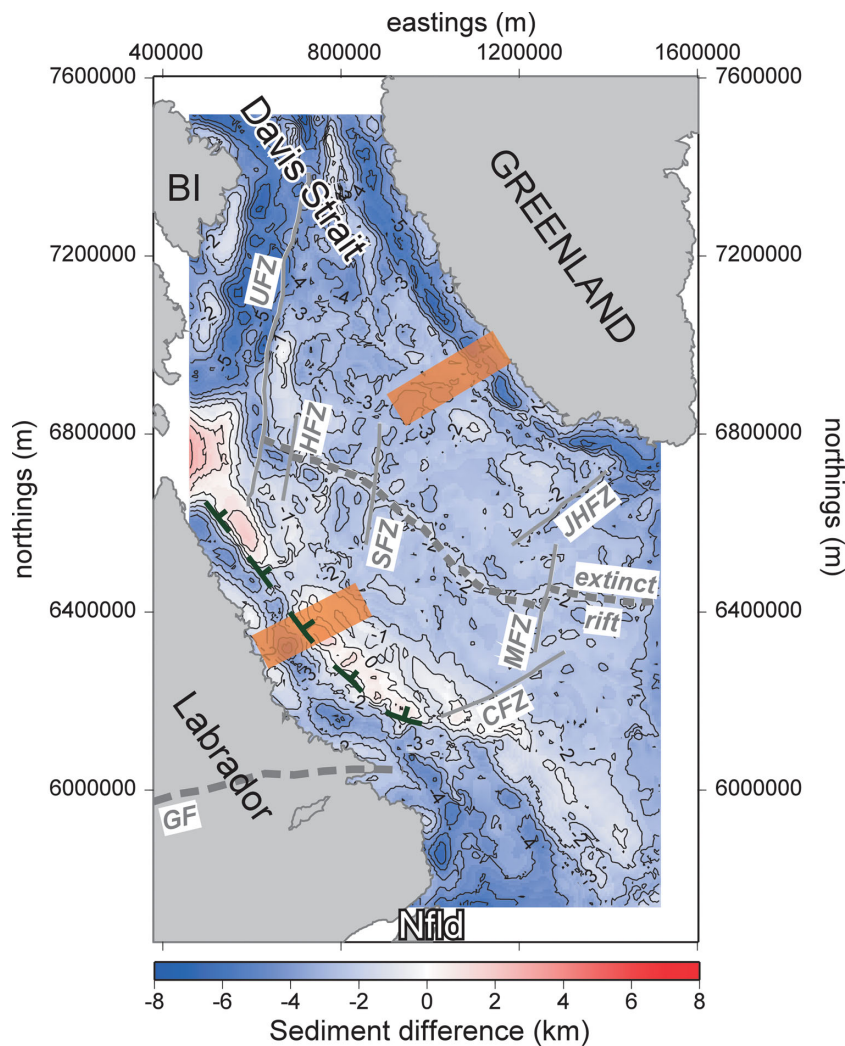


Figure 12. Sediment thickness difference map. Dark green fault symbols delineate interpreted southwestern edge of zone of graben bounding faults. The locations of the extinct rift (dashed grey line) and fracture zones (thin solid grey lines) within the Labrador Sea are plotted for reference. The orange boxes show the location of the non-volcanic to volcanic transition on both margins proposed by Keen *et al.* (2012). BI, Baffin Island; CFZ, Cartwright Fracture Zone; GF, Grenville Front; HFZ, Hudson Fracture Zone; JHFZ, Julian Haab Fracture Zone; MFZ, Minna Fracture Zone; SFZ, Snorri Fracture Zone; UFZ, Ungava Fault Zone.

thickness for a given crustal thickness with areas of sediment deficiency shown in blue and those of excess shown in red. Note that the choice of sediment density results in modest overcompensation in deep water. The added crustal thickness provided by anomalously high-density lower crust and underplates has not been considered in the calculation.

The main observation from Fig. 12 is that most of the Labrador Sea is moderately deficient in sediments. In contrast, the Hopedale Basin appears balanced while the Saglek Basin appears to have an excess of sediments. While Davis Strait appears to be particularly deficient in sediments (possibly because of the presence of an underplate that has not been included in the inferred crustal thickness), the Ungava Fault zone marks a sharp contrast in terms of the degree of that deficiency.

The margin-parallel zone of excess sediments in Fig. 12 appears to be unique to the Labrador margin and is bordered to the southwest by a strong gradient zone. As argued in Welford & Hall (2007), such geographically localized strong gradients can reveal steep listric faults in crust of finite flexural rigidity that is regionally supported and which doesn't satisfy local airy isostasy. The western

limit of this listric detachment or of a zone of multiple detachments is highlighted by the fault symbols in Fig. 12. In the top left corner of Fig. 13, the predicted sediment excess/deficiency from the listric detachment model from Welford & Hall (2007) has been superimposed on a thinned margin and used to predict the resulting free air gravity anomaly or 'edge effect'.

Watts & Marr (1995) investigated whether the free-air gravity anomaly 'edge effect' over rifted continental margins could be used as a first-order estimate of lithospheric strength. Using simple end-member flexural models from weak (elastic thickness, $T_e = 0$ km) to strong ($T_e = 25$ km), they computed the resulting free-air gravity anomaly 'edge effect' pattern and used it to estimate lithospheric strength across the east coast of the United States and around the margins of Africa. Strong margins were found to be associated with a broad, single-lobed high amplitude anomaly while weak margins were associated with shorter wavelength, low amplitude, double-lobed anomalies. For the African margins, Watts & Marr (1995) found that the length scale for lithospheric strength variations was on the order of several hundred kilometres and proposed that hot spot activity could be responsible for decreases in lithospheric strength.

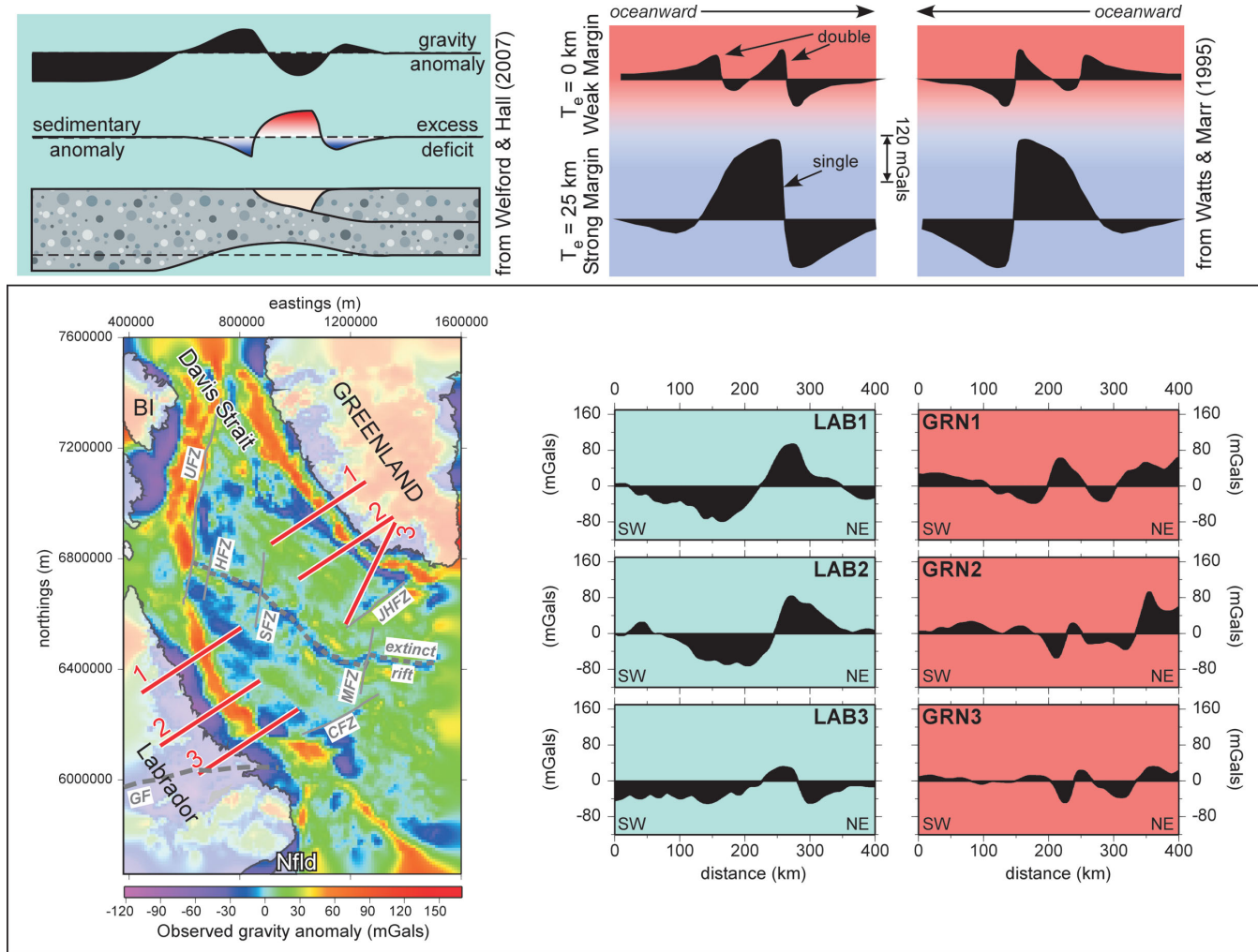


Figure 13. Comparison of free-air gravity anomaly ‘edge effect’ observed along six profiles from the Labrador and Greenland margins against the predicted anomaly over a graben bounding listric detachment from Welford & Hall (2007) and those from simple elastic flexural models from Watts & Marr (1995). The listric detachment model is shown to the top left with an arbitrary scale and the ‘edge effects’ computed from the end member models of Watts & Marr (1995) for weak margins (elastic thickness, $T_e = 0$ km) versus strong margins ($T_e = 25$ km) are plotted above the Labrador and Greenland profiles, at the same scale. Colour shading behind each of the Labrador and Greenland profiles corresponds with the interpreted style of margin. The locations of the extinct rift (dashed grey line) and fracture zones (thin solid grey lines) within the Labrador Sea are plotted for reference on the location map. BI, Baffin Island; CFZ, Cartwright Fracture Zone; GF, Grenville Front; HFZ, Hudson Fracture Zone; JHFZ, Julian Haab Fracture Zone; MFZ, Minna Fracture Zone; SFZ, Snorri Fracture Zone; UFZ, Ungava Fault Zone.

Using the listric detachment model from Welford & Hall (2007) and the end-member models from Watts & Marr (1995) for comparison, six free-air gravity anomaly profiles were extracted along the Labrador and Greenland margins (Fig. 13) in order to investigate the variations in the observed ‘edge effects’ and whether these could be used to infer crustal faulting and/or lithospheric strength.

For the Greenland margin, the gravity anomaly ‘edge effects’ are subdued and double-lobed, resembling the weak margin anomalies (highlighted in red) of Watts & Marr (1995). In contrast, while the Labrador margin ‘edge effects’ appear to more closely resemble those from the strong margin model (highlighted in blue) of Watts & Marr (1995), their polarities appear reversed with a pronounced gravity anomaly inboard rather than outboard of the single high. This pattern is more in line with the listric detachment model. Since the listric detachment model assumes finite, non-zero, flexural rigidity, some degree of lithospheric strength must be present on the Labrador margin and it is only the faulting style that causes the

predicted ‘edge effect’ from the strong margin end-member model of Watts & Marr (1995) to deviate from its idealized shape.

Regardless of faulting style, the ‘edge effect’ comparisons reveal that the lithosphere at the Greenland margin appears to be weaker than at the Labrador margin. This weakness may be due to far-field influence from the Iceland hotspot to the northeast (Lawver & Müller 1994) or to inherited variations in the lithospheric rheology. It is also possible that the strength variations are reflecting the presence of serpentinized mantle and the degree to which it has been serpentinized and consequently weakened (Escartín *et al.* 2001).

7 CONCLUSIONS

Constrained 3-D gravity inversions of the free air data over the Labrador Sea and its margins were undertaken to obtain regional density anomaly models, consistent with constraints obtained from seismic methods. The density anomaly isosurfaces that best fit seismic Moho constraints were selected as Moho-proxies and used, with

available sediment thickness estimates, to investigate variations in upper, middle, lower and total crustal thickness as well as variations in isostatic compensation. Key findings include:

(i) Moho depth generally corresponds to 12 km beneath the Labrador Sea but deepens to 20 km and greater towards Davis Strait and beneath the offshore extension of the Grenville Province.

(ii) Slices through the density anomaly models corresponding to seismic lines show good agreement between the inverted Moho-proxies and the seismic Moho, with the only exceptions occurring where a high velocity lower crustal zone or underplate has been modelled from WARRP studies.

(iii) Crust of the Labrador Sea is generally 5–10 km thick but thickens to 20–25 km towards Davis Strait and beneath the offshore extension of the Grenville Province, although these estimates do not include high density underplates or anomalously high density lower crust.

(iv) Assuming both uniform (35 km) and variable unstretched crustal thickness models, much of the Labrador Sea has experienced 70–90 per cent thinning.

(v) Stretching factor, β , values for the Labrador Sea derived from the inverted density anomaly models and depth to basement constraints suggest that embrittlement of the entire crust and serpentinization of the upper mantle are likely to have occurred for large portions of the central and southern Labrador Sea inboard of known oceanic crust. The northern limit of this zone roughly corresponds with the non-volcanic to volcanic transition zone recently proposed by Keen *et al.* (2012).

(vi) Sediment excess and deficiency on the Labrador and Greenland margins respectively, may be reflecting fundamental asymmetry in lithospheric strength with the Greenland margin appearing weaker than the Labrador margin. Lithospheric weakness of the Greenland margin may be due to inherited rheological variations, far-field influence from the Iceland hotspot to the northeast or possibly the presence and degree of serpentinization of mantle.

(vii) A strong margin-parallel gradient in the sediment excess and deficiency pattern on the Labrador margin may be revealing the southwestern limit of a regional graben bounding listric detachment or of a zone of distributed faults and detachments.

The inversion results provide a broad-scale 3-D view of the Labrador Sea and its margins that is consistent with results from previous seismic and geophysical studies and from which large-scale inferences can be made to better understand its evolution. It is hoped that the insights gleaned from this work will provide constraints for future regional palaeoreconstructions and may direct the focus of future geophysical investigations.

ACKNOWLEDGEMENTS

We would like to thank the Natural Sciences and Engineering Research Council of Canada for a Discovery Grant to Hall and Nalcor Energy for funding support of Welford. We would also like to thank John R. Hopper and an anonymous reviewer for their constructive comments.

REFERENCES

- Albertz, M., Beaumont, C., Shimeld, J., Ings, S. & Gradmann, S., 2010. An investigation of salt tectonic structural styles in the Scotia Basin, offshore Atlantic Canada: 1. Comparison of observations with geometrically simple numerical models, *Tectonics*, **29**(TC4017), doi:10.1029/2009TC002539.
- Andersen, O., Knudsen, P., Berry, P., Freeman, J., Pavlis, N. & Kenyon, S., 2008. The DNSC08 ocean wide altimetry derived gravity field, in *Proceedings of the EGU 2008 Meeting Programme*, Vienna, Austria, Abstract EGU2008-A-07163; G1-1MO10-003.
- Carter, J., Cameron, D., Wright, R. & Gillis, E., 2013. New insights on the slope and deep water region of the Labrador Sea, Canada, in *Proceedings of the EAGE Extended Abstracts*, London, U.K.
- Chalmers, J. & Pulvertaft, T., 2001. Development of the continental margins of the Labrador Sea: a review, *Geol. Soci. Spec. Publ.*, **187**, 77–105.
- Chalmers, J.A. & Laursen, K.H., 1995. Labrador Sea: the extent of continental and oceanic crust and the timing of the onset of seafloor spreading, *Mar. Petrol. Geol.*, **12**(2), 205–217.
- Chian, D. & Louden, K.E., 1992. The structure of Archean-Ketilidian crust along the continental shelf of southwestern Greenland from a seismic refraction profile, *Can. J. Earth Sci.*, **29**(2), 301–313.
- Chian, D. & Louden, K.E., 1994. The continent-ocean crustal transition across the southwest Greenland margin, *J. geophys. Res.*, **99**(B5), 9117–9135.
- Chian, D., Keen, C., Reid, I. & Louden, K.E., 1995a. Evolution of non-volcanic rifted margins: new results from the conjugate margins of the Labrador Sea, *Geology*, **23**(7), 589–592.
- Chian, D., Louden, K.E. & Reid, I., 1995b. Crustal structure of the Labrador Sea conjugate margin and implications for the formation of nonvolcanic continental margins, *J. geophys. Res.*, **100**(B12), 24 239–24 253.
- Dahl-Jensen, T. *et al.*, 2003. Depth to Moho in Greenland: receiver-function analysis suggests two Proterozoic blocks in Greenland, *Earth planet. Sci. Lett.*, **205**(3–4), 379–393.
- Dehler, S.A. & Welford, J.K., 2012. Variations in rifting style and structure of the Scotian margin, Atlantic Canada, from 3D gravity inversion, in *Conjugate Divergent Margins*, Vol. 369, eds Mohriak, W., Danforth, A., Post, P., Brown, D., Tari, G., Nemčok, M. & Sinha, S., Geological Society, London, Special Publications, doi:10.1144/SP369.11.
- Deptuck, M., MacRae, R., Shimeld, J., Williams, G. & Fensome, R., 2003. Revised upper Cretaceous and lower Paleogene lithostratigraphy and depositional history of the Jeanne d'Arc basin, offshore Newfoundland, Canada, *AAPG Bull.*, **87**, 1459–1483.
- Dickie, K., Keen, C.E., Williams, G.L. & Dehler, S.A., 2011. Tectonostratigraphic evolution of the Labrador margin, Atlantic Canada, *Mar. Petrol. Geol.*, **28**(9), 1663–1675.
- Divins, D., 2003. Total sediment thickness of the world's oceans & marginal seas, NOAA National Geophysical Data Center, Boulder, CO.
- Escrartín, J., Hirth, G. & Evans, B., 2001. Strength of slightly serpentinized peridotites: implications for the tectonics of oceanic lithosphere, *Geology*, **29**(11), 1023–1026.
- Funck, T. & Louden, K.E., 1998. Wide-angle seismic imaging of pristine Archean crust in the Nain Province, Labrador, *Can. J. Earth Sci.*, **35**, 672–685.
- Funck, T. & Louden, K.E., 1999. Wide-angle seismic transect across the Torngat Orogen, northern Labrador: evidence for a Proterozoic crustal root, *J. geophys. Res.*, **104**(B4), 7463–7480.
- Funck, T. & Louden, K.E., 2000. Wide-angle seismic imaging of a Mesoproterozoic anorthosite complex: the Nain Plutonic Suite in Labrador, Canada, *J. geophys. Res.*, **105**(B11), 25 693–25 707.
- Funck, T., Louden, K.E. & Hall, J., 2001a. Wide-angle reflectivity across the Torngat Orogen, NE Canada, *Geophys. Res. Lett.*, **28**(18), 3541–3544.
- Funck, T., Louden, K.E. & Reid, I., 2001b. Crustal structure of the Grenville Province in southeastern Labrador from refraction seismic data: evidence for a high-velocity lower crustal wedge, *Can. J. Earth Sci.*, **38**(10), 1463–1478.
- Funck, T., Jackson, H., Louden, K.E. & ofer, F.K., 2007. Seismic study of the transform-rifted margin in Davis Strait between Baffin Island (Canada) and Greenland: what happens when a plume meets a transform, *J. geophys. Res.*, **112**(4), doi:10.1029/2006JB004308.
- Funck, T., Hansen, A., Reid, I. & Louden, K.E., 2008. The crustal structure of the southern Nain and Makkovik provinces of Labrador derived from refraction seismic data, *Can. J. Earth Sci.*, **45**(4), 465–481.
- Gerlings, J., Funck, T., Jackson, H., Louden, K.E. & ofer, F.K., 2009. Seismic evidence for plume-derived volcanism during formation of the continental

- margin in southern Davis Strait and northern Labrador Sea, *Geophys. J. Int.*, **176**(3), 980–994.
- Gohl, K. & Smithson, S., 1993. Structure of Archean crust and passive margin of southwest Greenland from seismic wide-angle data, *J. geophys. Res.*, **98**, 6623–6638.
- Hall, J., Louden, K.E., Funck, T. & Deemer, S., 2002. Geophysical characteristics of the continental crust along the Lithoprobe Eastern Canadian Shield Onshore-Offshore Transect (ECSOOT): a review, *Can. J. Earth Sci.*, **39**, 569–587.
- Keen, C., Potter, P. & Srivastava, S., 1994. Deep seismic reflection data across the conjugate margins of the Labrador Sea, *Can. J. Earth Sci.*, **31**(1), 192–205.
- Keen, C.E., Dickie, K. & Dehler, S.A., 2012. The volcanic margins of the northern Labrador Sea: insights to the rifting process, *Tectonics*, **31**(TC1011), doi:10.1029/2011TC002985.
- Kristoffersen, Y. & Talwani, M., 1977. Extinct triple junction south of Greenland and the Tertiary motion of Greenland relative to North America, *Bull. geol. Soc. Am.*, **88**(7), 1037–1049.
- Lawver, L. & Müller, R.D., 1994. Iceland hotspot track, *Geology*, **22**(4), 311–314.
- Li, Y. & Oldenburg, D.W., 1996. 3-D inversion of magnetic data, *Geophysics*, **61**(2), 394–408.
- Li, Y. & Oldenburg, D.W., 1998. 3-D inversion of gravity data, *Geophysics*, **63**, 109–119.
- Louden, K., Tucholke, B. & Oakey, G., 2004. Regional anomalies of sediment thickness, basement depth and isostatic crustal thickness in the North Atlantic Ocean, *Earth planet. Sci. Lett.*, **224**(1–2), 193–211.
- Louden, K.E., Osler, J., Srivastava, S. & Keen, C., 1996. Formation of oceanic crust at slow spreading rates: new constraints from an extinct spreading center in the Labrador Sea, *Geology*, **24**(9), 771–774.
- Oakey, G. & Stark, A., 1995. A digital compilation of depth to basement and sediment thickness for the North Atlantic and adjacent coastal land areas, Open file #3039, 29pp., Geological Survey of Canada.
- Osler, J. & Louden, K.E., 1992. Crustal structure of an extinct rift axis in the Labrador Sea: preliminary results from a seismic refraction survey, *Earth planet. Sci. Lett.*, **108**(4), 243–258.
- Osler, J. & Louden, K.E., 1995. Extinct spreading center in the Labrador Sea: crustal structure from a two-dimensional seismic refraction velocity model, *J. geophys. Res.*, **100**(B2), 2261–2278.
- Pérez-Gussinyé, M. & Reston, T., 2001. Rheological evolution during extension at nonvolcanic rifted margins: onset of serpentization and development of detachments leading to continental breakup, *J. geophys. Res.*, **106**(B3), 3961–3975.
- Pérez-Gussinyé, M., Ranero, C., Reston, T. & Sawyer, D., 2003. Mechanisms of extension at nonvolcanic margins: evidence from the Galicia interior basin, west of Iberia, *J. geophys. Res.*, **108**(B5), doi:10.1029/2001JB000901.
- Reid, I., 1996. Crustal structure across the Nain-Makkovik boundary on the continental shelf off Labrador from seismic refraction data, *Can. J. Earth Sci.*, **33**(3), 460–471.
- Reston, T., 2007. Extension discrepancy of North Atlantic nonvolcanic rifted margin: depth-dependent stretching or unrecognized faulting?, *Geology*, **35**(4), 367–370.
- Roest, W. & Srivastava, S., 1989. Sea-floor spreading in the Labrador Sea: a new reconstruction, *Geology*, **17**(11), 1000–1003.
- Sandwell, D.T. & Smith, W.H., 1997. Marine gravity anomaly from Geosat and ERS 1 satellite altimetry, *J. geophys. Res.*, **102**(B5), 10 039–10 054.
- Sinclair, I. & Withjack, M., 2008. Mid to Late Cretaceous structural and sedimentary architecture at the Terra Nova Oilfield, offshore Newfoundland—implications for the tectonic history of the North Atlantic, in *Central Atlantic Conjugate Margins*, pp. 125–141, ed. Brown, D., Dalhousie University.
- Sørensen, A., 2006. Stratigraphy, structure and petroleum potential of the Lady Franklin and Maniitsoq Basins, offshore southern SW Greenland, *Petrol. Geosci.*, **12**, 221–234.
- Srivastava, S., 1978. Evolution of the Labrador Sea and its bearing on the early evolution of the North Atlantic, *Geophys. J. R. astr. Soc.*, **52**(2), 313–357.
- Srivastava, S. & Keen, C., 1995. A deep seismic reflection profile across the extinct Mid-Labrador Sea spreading center, *Tectonics*, **14**, 372–389.
- Srivastava, S. & Roest, W., 1999. Extent of oceanic crust in the Labrador Sea, *Mar. Petrol. Geol.*, **16**(1), 65–84.
- van der Linden, W., 1975. Crustal attenuation and sea-floor spreading in the Labrador Sea, *Earth planet. Sci. Lett.*, **27**(3), 409–423.
- Watts, A. & Marr, C., 1995. Gravity anomalies and the thermal and mechanical structure of rifted continental margins, in *Rifted Ocean-Continent Boundaries*, Vol. 463, pp. 65–94, eds Banda, E., Torné, M. & Talwani, M., NATO ASI Series, Series C: Mathematical and Physical Sciences, Kluwer Academic Publishers.
- Welford, J.K. & Hall, J., 2007. Crustal structure across the Newfoundland rifted continental margin from constrained 3-D gravity inversion, *Geophys. J. Int.*, **171**, 890–908.
- Welford, J.K., Shannon, P.M., O'Reilly, B.M. & Hall, J., 2010. Lithospheric density variations and Moho structure of the Irish Atlantic continental margin from constrained 3-D gravity inversion, *Geophys. J. Int.*, **183**(1), 79–95.
- Welford, J.K., Shannon, P.M., O'Reilly, B.M. & Hall, J., 2012. Comparison of lithosphere structure across the Orphan Basin-Flemish Cap and Irish Atlantic conjugate continental margins from constrained 3D gravity inversions, *J. geol. Soc. Lond.*, **169**(4), 405–420.